machines

MDPI

Article

Discrete-Time Adaptive Decentralized Control for Interconnected Multi-Machine Power Systems with Input Quantization

Junxiong Ge [1], Mengyun Wang [2], Haimin Hong [3], Jinyu Zhao [4], Guowei Cai [1], Xiuyu Zhang [1,*] and Pukun Lu [1,*]

[1] Department of Electrical Engineering, Northeast Electric Power University, Jilin 132012, China
[2] Jilin Provincial International Joint Research Center of Precision Drive and Intelligent Control, Northeast Electric Power University, Jilin 132012, China
[3] Department of Electrical Engineering, Tsinghua University, Beijing 100084, China
[4] Shenzhen Guodian Technology Communication Company Ltd., Shenzhen 518000, China
* Correspondence: zhangxiuyu80@163.com (X.Z.); loopkun@163.com (P.L.)

Abstract: This study contrives a discrete-time adaptive decentralized control algorithm with input quantization for interconnected multi-machine power systems with SVC. First, a dynamic surface scheme is applied to the excitation controller design, in which first-order digital low-pass filters are used to predict the next virtual control law, which overcomes the model conversion problem in backstepping. Therefore, the controller design and structure are simplified. Further, an improved hysteresis quantizer is utilized for amplitude quantization of control input signals; along with the discretization of time, this achieves digital decentralized control. Finally, semi-global uniformly ultimately boundedness (SGUUB) of the whole control system is demonstrated based on the Lyapunov stability theory, and the effectiveness of the proposed control algorithm is verified on the ModelingTech real-time simulation experimental platform for power electronics.

Keywords: multi-machine power systems; adaptive decentralized control; discrete-time; dynamic surface control; hysteresis quantizer

Citation: Ge, J.; Wang, M.; Hong, H.; Zhao, J.; Cai, G.; Zhang, X.; Lu, P. Discrete-Time Adaptive Decentralized Control for Interconnected Multi-Machine Power Systems with Input Quantization. *Machines* **2022**, *10*, 878. https://doi.org/10.3390/machines10100878

Academic Editor: Alejandro Gómez Yepes

Received: 31 August 2022
Accepted: 23 September 2022
Published: 29 September 2022

1. Introduction

At the beginning of this century, power systems entered a new stage of development. The integration of multiple new energy sources and the increase in load equipment types make power system more complex (such as strong nonlinear characteristics, strong coupling characteristics, etc.), which brings new challenges to power system stability control [1–6]. The effective way to deal with the stability of a large-scale power system is to use advanced control theory to design controllers, such as generator excitation control, flexible AC transmission technology control, steam turbine speed control, and so on [7,8]. Generator excitation control has an excellent effect on improving the damping characteristics and stability of power system and is the most frequently used method [9–13]. In [12], for a multi-machine power system with unknown nonlinear dynamics, the author uses a nonlinear recursive algorithm to design an excitation controller, which improves the robustness of the system in the presence of measurement errors.

From the aspect of decentralized control theory, with the expansion of total installed capacity and a large-area interconnected power grid, the traditional linear control method is only effective for small external disturbances near the equilibrium point, and the feedback signal of each subsystem is difficult to collect in time and accurately, which makes the practical application of a centralized controller difficult [14]. To address these problems, Ref. [15] proposed a decentralized adaptive control scheme for the first time. Following the study of P. Ioannou, adaptive decentralized control strategy has been widely studied and applied, such as in [16–22]. In [21], for interconnected power systems, a decentralized robust load frequency controller was designed. In [23], time delays were considered.

It should be noted that all the above works are almost always developed in continuous time, and controller design based on continuous-time systems have made great progress and achievements [24–28]. However, in modern industrial production processes, controllers are almost always based on microprocessors to achieve digital control, such as single-chip microcomputers, DSP, PLC, etc. This means that a controller based on a continuous-time system must be converted into a digital signal through A/D and D/A to achieve control. However, due to the impact of sampling time, when a continuous-time control algorithm is implemented on a digital device, control performance is reduced or even invalid. Therefore, it is necessary and feasible to construct a discrete-time model of the controlled system and design a discrete-time controller [29–31].

In [29], for the first time, Yeh and Kokotovic designed an adaptive controller for a class of SISO discrete-time systems to ensure tracking performance and avoid the shortcomings of over-parameterization. Since then, by combining with fuzzy or neural networks, adaptive backstepping control schemes have been proposed for discrete-time systems, which significantly simplifies the controller design process for nonlinear systems [32–35]. For a class of single-input–single-output discrete-time systems with parameter uncertainties, in [36], an adaptive controller is designed using the state prediction, which eliminates the influence of parameter uncertainties and achieves accurate global output tracking. In order to deal with the unknown functions in a controlled system, fuzzy logic systems and neural networks are favored by scholars around the world because of their inherent universal approximation characteristics, and they have been widely used in the intelligent controller design process of discrete-time nonlinear systems [37–39].

Quantized control schemes, as an effective means to realize digital control, play an important role in computer-based intelligent control systems and are widely used in modern digital control and network control systems because they can produce sufficient accuracy and reduce communication rate. In [40,41], a quantized backstepping control scheme was designed for a class of nonlinear systems, in which both the quantized effect and input nonlinearity were taken into consideration. In [42], by considering the quantization of state measurement signals and the control input signal, a quantized output feedback control strategy was designed for a class of discrete-time systems, and the prescribed H_∞ performance of the closed-loop system was achieved. In [27,43], a novel hysteretic quantizer was introduced to the control system design for a class of nonlinear systems which had been introduced for its interconnectedness. The quantizer parameters are adjusted freely with dynamic changes to the tracking error and communication burden, which significantly improves the efficiency of the control system and the stability of he closed-loop system. Because of its norm estimation, the number of adjustable parameters is reduced to two, which simplifies controller design. One noteworthy fact is that the above-mentioned research overcomes the non-causal problem by transforming the system into a special form and makes it suitable for backstepping, which increases the complexity of controller design and stability analysis of discrete-time systems. There is still a lot of research space to be explored.

Motivated by the above discussion, in this paper, a discrete-time adaptive decentralized neural excitation controller with input quantization for interconnected multi-machine power systems is developed. Compared with existing related research work, the main features are as follows:

(1) The original system model does not need to be converted into an unknown special form, as we use dynamic surface control with a digital first-order low-pass filter at each step. Compared with backstepping control, digital first-order low-pass filters have been introduced to overcome the "explosion of complexity" in the proposed method and to avoid system conversions. Further, RBFNNs are employed to approximate the unknown nonlinear terms in the system. Therefore, the design and structure of the controller are simplified.

(2) An improved hysteresis quantizer is employed to quantize the control input signal amplitudes, which can reduce the number of transformations and reduce chattering

compared to methods that do not use a hysteresis quantizer. Together with the discretization of time, digital control is practically realized. The transmission of a digital signal can effectively suppress noise, thus significantly improving the anti-interference ability of the power system. Because of the transmission delay of the power system, it is easier to stabilize by introducing sampling.

(3) The ModelingTech real-time simulation experiment platform for power electronics is used in this study to verify the utility of the proposed control strategy with input quatization. On the hardware-in-loop experimental platform, the controller and the model of the two-machine power system can run on different devices, and the signals are transmitted through the data transmission channel; the control of interconnected multi-machine power systems with input quantization is solved. Thus, the power system is tested and verified very similarly to the real situation.

2. System Description and Preliminaries

2.1. Multi-Machine Power System Model

The meanings of the main symbols are given in the Table 1.

Table 1. Notation for multi-machine power systems.

Symbol	Nomenclature	Symbol	Nomenclature
δ_i	Power angle of the ith generator, in rad	ω_i	Relative speed of the ith generator, in rad/s
f_0	Rated frequency, in Hz	ω_0	Synchronous machine speed, in rad/s
D_i	Per-unit damping constant	P_{mi}	Mechanical input power, in p.u.
H_i	Inertia constant, in seconds	P_{ei}	Electrical power, in p.u.
E'_{qi}	Q-axis internal transient electric potential, in p.u.	E_{qi}	EMF in the quadrature axis, in p.u.
E_{fi}	Equivalent EMF in the excitation coil, in p.u.	k_{ei}	Gain of the excitation amplifier, in p.u.
u_{fi}	Input of the SCR amplifier, in p.u.	x_{adi}	Mutual reactance between the excitation coil and the stator coil, in p.u.
T'_{d0i}	Direct axis transient short-circuit time constant, in seconds	Q_{ei}	Reactive power, in p.u.
I_{qi}	Quadrature axis current, in p.u.	I_{di}	Direct axis current, in p.u.
B_{ij}	The *ith* row and *jth* column element of nodal susceptance matrix at the internal nodes after eliminating all physical buses, in p.u.	x_{di}	Direct axis reactance, in p.u.
x'_{di}	Direct axis transient reactance, in p.u.	T_{ci}	Time constant of adjusting system and SVC, in p.u.
u_{Bi}	Input of SVC, in p.u.	B_{Li}	Adjustable equivalent susceptance in SVC, in p.u.
B_{Ci}	Initial value of adjustable susceptance, in p.u.	V_{mi}	Access point voltage of SVC, in p.u.
V_{refi}	Reference of accessing point voltage of SVC, in p.u.		

The mathematical model of multi-machine power systems with n generators interconnected by a transmitted network and equipped with SVC is obtained using the method shown in [10]:

$$\begin{aligned}
\dot{\delta}_i(t) &= \omega_i, \\
\dot{\omega}_i(t) &= \frac{\omega_0}{2H_i}(P_{mi} - P_{ei}) - \frac{D_i}{2H_i}\omega_i(t) + d_i, \\
\dot{E}'_{qi}(t) &= \frac{1}{T'_{d0i}}\Big[E_{fi}(t) - E_{qi}(t)\Big],
\end{aligned} \tag{1}$$

where $i = 1, \cdots, n$. After formula derivation, we obtain the equation as follows. Please see the Appendix for a detailed Proof.

$$\begin{aligned}
\dot{x}_{i1} &= x_{i2},\\
\dot{x}_{i2} &= \theta_{i2}x_{i2} - g_{i2}x_{i3} + d_i,\\
\dot{x}_{i3} &= \theta_{i3}x_{i3} + g_{i3}u_i + \gamma_i(\delta,\omega),\\
y_{i1} &= x_{i1}. \qquad (2)\\
\dot{x}_{i4} &= g_{i4}u'_{Bi} + f_{i4}(\bar{x}_{i4}),\\
y_{i2} &= x_{i4}. \qquad (3)
\end{aligned}$$

where y_{i1} and y_{i2} are the output signals, and $\theta_{i2} = -\frac{D_i}{2H_i}$, $\theta_{i3} = -\frac{1}{T'_{d0i}}$, $g_{i2} = \frac{\omega_0}{2H_i}$, $g_{i3} = \frac{1}{T'_{d0i}}$, $g_{i4} = \frac{X_{1i}X_{2i}}{T_{ci}X'_{d\Sigma i}}$, $u'_{Bi} = -x_{i4}u_{Bi}$, $f_{i4}(\bar{x}_{i4}) = -\frac{\sin x_{i1}X_{1i}X_{2i}}{(x_{i4}+V_{refi})(X'_{d\Sigma i})^2}x_{i2}E'_{qi} - \frac{X_{1i}X_{2i}(x_{i4}+V_{refi})}{X'_{d\Sigma i}T_{ci}}(-B_{Li} + B_{Ci}) + \frac{X_{2i}^2E'_{qi}+X_{1i}X_{2i}\cos x_{i1}}{(x_{i4}+V_{refi})(X'_{d\Sigma i})^2}(-\frac{X_{d\Sigma i}}{T_{d0i}X'_{d\Sigma i}}E'_{qi} + \frac{1}{T_{d0i}}\frac{X_{di}-X'_{di}}{X'_{d\Sigma i}}\cos x_{i1}) + \frac{X_{2i}^2x_{i3}+X_{1i}X_{2i}V_{si}\cos\delta_i}{T_{d0i}V_{mi}(X'_{d\Sigma i})^2}u_i$.

Similar to [39], by using the Euler method, the interconnected multi-machine power systems (2) and (3) are discretized, and the dynamic model in discrete-time form can be obtained as follows:

$$\begin{aligned}
x_{i1}(k+1) &= x_{i1}(k) + \Delta_t x_{i2}(k),\\
x_{i2}(k+1) &= (1+\Delta_t\theta_{i2})x_{i2}(k) - \Delta_t g_{i2}x_{i3}(k) + \Delta_t d_i(k),\\
x_{i3}(k+1) &= (1+\Delta_t\theta_{i3})x_{i3}(k) + \Delta_t g_{i3}Q(u_i(k))\\
&\quad + \Delta_t\textstyle\sum_{j=1}^{n}\delta_{ji}(|x_{i1}|,|x_{i2}|),\\
y_{i1}(k) &= x_{i1}(k). \qquad (4)
\end{aligned}$$

$$\begin{aligned}
x_{i4}(k+1) &= x_{i4}(k) + \Delta_t g_{i4}Q\big(u'_{Bi}(k)\big) + \Delta_t f_{i4}(\bar{x}_{i4}),\\
y_{i2}(k) &= x_{i4}(k). \qquad (5)
\end{aligned}$$

The control objective in this paper is to design a neural network-based decentralized digital dynamic surface excitation control scheme for a multi-machine power system with SVC (1), (A1), and (A2), and to ensure all the signals of the closed loop are ultimately bounded and converge the tracking error into an arbitrarily small neighborhood of the origin.

2.2. Hysteresis Quantizer Description

Similar to the literature [27], the description of the hysteresis quantizer we use is as follows.

$$Q_i(u_i) = \begin{cases} p_{i,j}, & \text{if } \frac{p_{i,j}}{1+\delta_i} < u_i \le p_{i,j},\ Q_i^- \ge p_{i,j},\\ & \text{or } p_{i,j} \le u_i < \frac{p_{i,j}}{1-\delta_i},\ Q_i^- \le p_{i,j},\\ (1+\delta_i)p_{i,j}, & \text{if } p_{i,j} < u_i \le \frac{p_{i,j}}{1-\delta_i},\\ & \quad Q_i^- \ge (1+\delta_i)p_{i,j},\\ & \text{or } \frac{p_{i,j}}{1-\delta_i} \le u_i < p_{i,j+1},\\ & \quad Q_i^- \le (1+\delta_i)p_{i,j},\\ 0, & \text{if } 0 \le u_i \le \frac{p_{i,1}}{1+\delta_i},\\ & \text{or } \frac{p_{i,1}}{1+\delta_i} < u_i < p_{i,1}, Q_i^- = 0,\\ -Q_i(-u_i), & \text{if } u_i < 0. \end{cases} \qquad (6)$$

where $\delta_i = (1-\varepsilon_i(t))/(1+\varepsilon_i(t)), 0 < \varepsilon_i(t) < 1, p_{i,j} = a_i(t)\varepsilon_i^{1-j}(t), a_i(t) > 0, j = 1,2,3\cdots$. The parameter $a_i(t)$ determines the size of the dead-zone for $Q_i(u_i)$, and $\varepsilon_i(t)$ is a measure of quantitative density. The smaller $\varepsilon_i(t)$ is, the coarser the quantizer. In Formula (6), $Q_i^-(t)$ is the latest value of Q_i, and $Q_i^-(0) := 0$. When $t \in [0, T_{i,1}]$, there is $Q_i^-(t) = 0$, and $Q_i^-(t) = Q_i(u_i(T_{i,h}))$ for $t \in [T_{i,h}, T_{i,h+1}]$, where $T_{i,h}(h = 1,2,3\cdots), 0 < T_{i,1} < T_{i,2} < T_{i,3} < \cdots < +\infty$ denotes the current time of $Q_i(u_i)$ conversion. When $u > 0$, Formula (6) is drawn as in Figure 1.

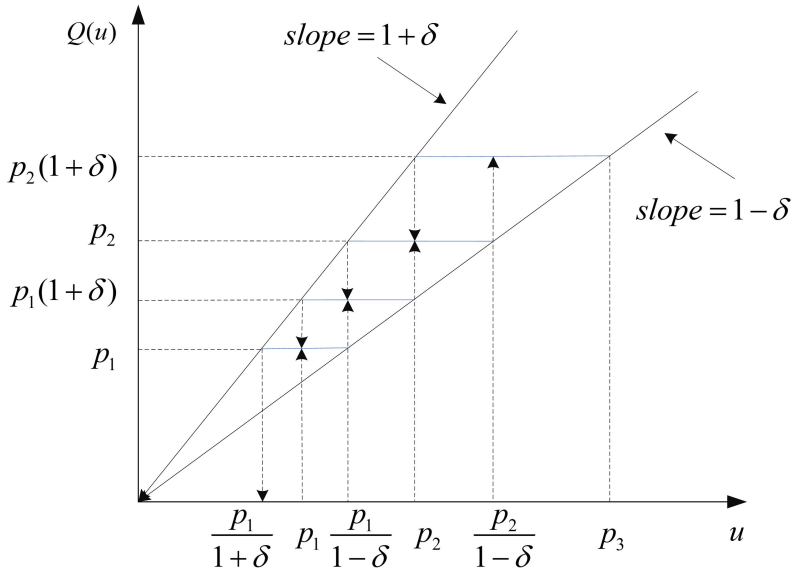

Figure 1. Hysteresis quantizer.

Different from existing quantization methods, such as [14,44], the parameters of the quantizer are assumed to be certain constants or parameters from the literature [45], and the quantizer can be changed, but some included inequalities still need to be satisfied.

Remark 1. *Figure 1 expresses the mathematical relation for Equation (6), and there are no units on either axis. The hysteresis quantizer is introduced in this paper; it can decrease the number of transitions and reduce the chattering phenomena.*

In the entire operation program, let the maximum values of $a_i(t)$ and $\varepsilon_i(t)$ be represented as $\bar{a}_i$ and $\bar{\varepsilon}_i$, and the minimum values are represented as $\underline{a}_i$ and $\underline{\varepsilon}_i$; we can get

$$0 < \underline{a}_i \le a_i(t) \le \bar{a}_i, 0 < \underline{\varepsilon}_i \le \varepsilon_i(t \le \bar{\varepsilon}_i < 1, \ \forall t \ge 0. \tag{7}$$

By use of the Euler method, as in the literature [39], the discrete-time dynamic model of a multi-machine power system can be described as follows:

$$\begin{aligned} x_{i1}(k+1) &= x_{i1}(k) + \Delta_t x_{i2}(k), \\ x_{i2}(k+1) &= (1 + \Delta_t \theta_{i2}) x_{i2}(k) - \Delta_t g_{i2} x_{i3}(k) + \Delta_t d_i(k), \\ x_{i3}(k+1) &= (1 + \Delta_t \theta_{i3}) x_{i3}(k) + \Delta_t g_{i3} Q(u_i(k)) \\ &\quad + \Delta_t \textstyle\sum_{j=1}^{n} \delta_{ji}(|x_{i1}|, |x_{i2}|), \\ y_{i1}(k) &= x_{i1}(k). \end{aligned} \tag{8}$$

$$\begin{aligned} x_{i4}(k+1) &= x_{i4}(k) + \Delta_t g_{i4} Q\big(u'_{Bi}(k)\big) + \Delta_t f_{i4}(\bar{x}_{i4}), \\ y_{i2}(k) &= x_{i4}(k). \end{aligned} \tag{9}$$

2.3. RBF Neural Networks (RBFNNs)

In this paper, the approximation property of RBF neural networks is used to approximate the unknown continuous function $h_{ij}(\xi_j)$ with the following form [38]:

$$h_{ij}(\xi_{ij}) = \eta_{ij}^T \psi_{ij}(\xi_{ij}), \tag{10}$$

where $\xi_{ij} = \left[\xi_{ij}^1, ..., \xi_{ij}^p\right] \in R^p$ is the input of the RBFNN, $\eta_{ij} = \left[\eta_{ij}^1, ..., \eta_{ij}^m\right]^T \in R^m$ is the weight vector, with m being the RBFNN node number, $\psi_{ij}(\xi_{ij}) = \left[\psi_{ij}^1(\xi_{ij}), ..., \psi_{ij}^m(\xi_{ij})\right]^T \in R^m$ is the Gaussian basis function with the following form

$$\psi_{ij}^l(\xi_{ij}(k)) = \exp\left[-\frac{\left\|\xi_{ij} - c_{ijl}\right\|}{2b_{ijl}^2}\right], l = 1, ..., m, \tag{11}$$

with $c_{ijl} = \left[c_{ijl}^1, ..., c_{ijl}^p\right]^T$ the center of the Gaussian function, and $b_{ijl} \in R$ is the width. Then, (10) can be rewritten as

$$h_{ij}(\xi_{ij}) = \eta_{ij}^{*T}\psi_{ij}(\xi_{ij}) + \varepsilon_{ij}(\xi_{ij}), \tag{12}$$

where η_{ij}^{*T}, $\varepsilon_{ij}(\xi_{ij})$ are the ideal weight vector and the optimal approximation error, respectively, and have the following property: define $\left\|\psi_{ij}(\xi_{ij})\right\|^2 \leq l_{ij}$, and $|\varepsilon_{i2}(\xi_{i2}(k))| \leq \bar{\varepsilon}_{ij}$, with l_{ij} and $\bar{\varepsilon}_{ij}$ positive constants when ξ_{ij} belongs to a compact set $\Omega_{\xi_{ij}}$. For the controlled (8) and (9), the following assumption are necessary [46].

Assumption 1. *The reference signal y_{ri} is smooth and bounded; for $k > 0$, $[y_{ri}(k), y_{ri}(k+1), y_{ri}(k+2)]$ belongs to a compact set Ω_r.*

Assumption 2. *The composite interference signal d_i is bounded, and there is a positive constant $\bar{d}_i$ such that $|d_i(k)| \leq \bar{d}_i$.*

There exist two positive constants $\underline{g}_{ij}$ and $\bar{g}_{ij}$ such that $\underline{g}_{ij} \leq \left|g_{ij}\right| \leq \bar{g}_{ij}, i = 1, 2, \cdots, n$, $j = 2, 3,$, and the disturbance d_i is bounded, which satisfies $|d_i(k)| \leq \bar{d}_i$.

Remark 2. *Since the reference signal y_{ri} is always bounded, and g_{ij} are unknown constants, Assumptions 1 and 2 are reasonable, and they are common assumptions in dynamic surface control methods [46].*

The control objective in this paper is to design a neural network-based decentralized digital dynamic surface excitation control scheme for multi-machine power systems with SVC (1), (A1), and (A2), ensuring all the signals of the closed loop are ultimately bounded and converge the tracking error into an arbitrarily small neighborhood of the origin.

Remark 3. *In fact, in this paper, an RBFNN is used to estimate the unknown continuous function; the weight vector of the RBFNN is updated by the adaptive laws during the simulation. The adaptive laws are influenced by the inputs and states of the system. Thus, the RBFNN is learning online instead of learning offline.*

3. Discrete-Time Decentralized Controller Scheme

The discrete-time decentralized adaptive dynamic surface quantized control (DDAD-SCQC) scheme for interconnected multi-machine systems with SVC is addressed. First, due to the drawbacks of traditional backstepping, digital first-order low-pass filters are introduced at the second and third steps to avoid coordinate transformation of the mathematical model. Next, the improved hysteresis quantizer is utilized to reduce chattering. Finally, RBFNNs are employed to reconstruct the unknown nonlinear terms. The control structure diagram is shown in Figure 2. Following is the detailed controller design.

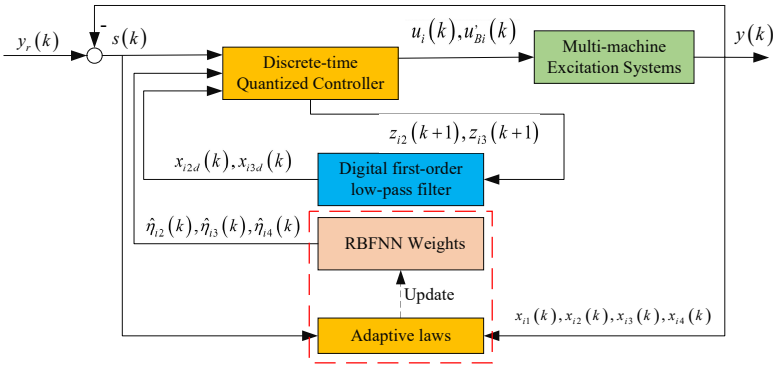

Figure 2. Structure diagram of the proposed control scheme.

Step 1: Define s_{i1} as the first tracking error surface

$$s_{i1}(k) = x_{i1}(k) - y_{ri}(k) \tag{13}$$

where y_{ri} is the reference signal of the ith subsystem. From (8), we can obtain

$$\begin{aligned} s_{i1}(k+1) &= x_{i1}(k+1) - y_{ri}(k+1) \\ &= x_{i1}(k) + \Delta_t x_{i2}(k) - y_{ri}(k+1). \end{aligned} \tag{14}$$

Then, choose the virtual control $x_{i2d}(k)$ as

$$x_{i2d}(k) = \frac{k_{i1}}{\Delta_t}[-x_{i1}(k) + y_{ri}(k+1)]. \tag{15}$$

Let $x_{i2d}(k)$ pass through the following first-order filter to obtain a new state variable $z_{i2}(k)$:

$$\tau_{i2} z_{i2}(k+1) + b_{i2} z_{i2}(k) = x_{i2d}(k),\ z_{i2}(0) = x_{i2d}(0) \tag{16}$$

where τ_{i2} is the time constant, and b_{i2} is a positive parameter.

Step 2: The second error surface $s_{i2}(k)$ is defined as

$$s_{i2}(k) = xinx_{i2}(k) - z_{i2}(k). \tag{17}$$

From the second equation of (8), the first difference of $s_{i2}(k)$ yields

$$\begin{aligned} s_{i2}(k+1) &= x_{i2}(k+1) - z_{i2}(k+1) \\ &= (1 + \Delta_t \theta_{i2}) x_{i2}(k) - \Delta_t g_{i2} x_{i3}(k) \\ &\quad + \Delta_t d_i(k) - z_{i2}(k+1). \end{aligned} \tag{18}$$

Let:

$$h_{i2}(k) = -\frac{1}{\Delta_t g_{i2}}[(1 + \Delta_t \theta_{i2}) x_{i2}(k) + \Delta_t d_i(k) - z_{i2}(k+1)]. \tag{19}$$

Noting that $h_{i2}(k)$ contains the external disturbance $d_i(k)$ and uncertain parameters g_{i2} and θ_{i2}, this increases the complexity of the controller structure and makes controller design more difficult. Therefore, an RBF neural network is introduced to estimate the unknown nonlinear term $h_{i2}(k)$ online:

$$h_{i2}(k) = \eta_{i2}^{*T} \psi_{i2}(\xi_{i2}(k)) + \varepsilon_{i2}(\xi_{i2}(k)), \tag{20}$$

which has characteristics such as $\|\psi_{i2}(\xi_{i2}(k))\|^2 \leq l_{i2}$, $|\varepsilon_{i2}(\xi_{i2}(k))| \leq \bar{\varepsilon}_{i2}$ and $\xi_{i2}(k) = [\bar{x}_{i2}(k), x_{i2d}(k), z_{i2}(k)]^T \in \Omega_{\xi_{i2}}$ and is the input vector of the RBFNN. Let $\hat{\eta}_{i2}(k)$ be the

estimate of η_{i2}^*, and $\tilde{\eta}_{i2}(k) = \hat{\eta}_{i2}(k) - \eta_{i2}^*(k)$. Now, the second virtual control law $x_{i3d}(k)$ and adaptive law $\hat{\eta}_{i2}(k+1)$ can be chosen as

$$x_{i3d}(k) = k_{i2}s_{i2}(k) + k_{i2}\hat{\eta}_{i2}^T(k)\psi_{i2}(\xi_{i2}(k)), \tag{21}$$

$$\begin{aligned}\hat{\eta}_{i2}(k+1) = \hat{\eta}_{i2}(k) - \lambda_{i2}(\psi_{i2}(\xi_{i2}(k))s_{i2}(k+1) \\ + \sigma_{i2}\hat{\eta}_{i2}(k)),\end{aligned} \tag{22}$$

where k_{i2}, λ_{i2}, and σ_{i2} are the positive design parameters. Similar to [47], there are no rules or limitations in the process of controller design, and the ultimate goal is to satisfy the Lyapunov stability condition. According to (22), the following formula is available

$$\begin{aligned}\tilde{\eta}_{i2}(k+1) = \tilde{\eta}_{i2}(k) - \lambda_{i2}(\psi_{i2}(\xi_{i2}(k))s_{i2}(k+1) \\ + \sigma_{i2}\hat{\eta}_{i2}(k)).\end{aligned} \tag{23}$$

Let $x_{i3d}(k)$ pass through a first-order filter to obtain a new state variable $z_{i3}(k)$,

$$\tau_{i3}z_{i3}(k+1) + b_{i3}z_{i3}(k) = x_{i3d}(k),\ z_{i3}(0) = x_{i3d}(0) \tag{24}$$

where τ_{i3} is the time constant, and b_{i3} is a positive parameter.

Step 3: Define the third error surface $s_{i3}(k)$,

$$s_{i3}(k) = x_{i3}(k) - z_{i3}(k). \tag{25}$$

According to (8), the first difference of $s_{i3}(k)$ is

$$\begin{aligned}s_{i3}(k+1) &= x_{i3}(k+1) - z_{i3}(k+1) \\ &= (1 + \Delta_t\theta_{i3})x_{i3}(k) + \Delta_t g_{i3}Q(u_i(k)) \\ &+ \Delta_t\textstyle\sum_{j=1}^{n}\delta_{ji}(|x_{i1}|, |x_{i2}|) - z_{i3}(k+1)\end{aligned} \tag{26}$$

where $Q(u_i(k))$ has been described in (6); define

$$\iota_{i1}(k) = \begin{cases} \frac{Q(u_i(k))}{u_i(k)}, & \text{if } |u_i(k)| \geq a(k), \\ 1, & \text{if } |u_i(k)| < a(k), \end{cases} \tag{27}$$

$$\iota_{i2}(k) = \begin{cases} 0, & \text{if } |u_i(k)| \geq a(k), \\ Q(u_i(k)) - u_i(k), & \text{if } |u_i(k)| < a(k). \end{cases} \tag{28}$$

Then, the quantizer (6) can be rewritten as:

$$Q(u_i(k)) = \iota_{i1}(k)u_i(k) + \iota_{i2}(k). \tag{29}$$

As described in [27], the following inequality can be obtained

$$1 - \delta \leq \tfrac{Q(u_i(k))}{u_i(k)} \leq 1 + \delta,\ \text{if } |u_i(k)| \geq a(k), \tag{30}$$

$$|Q(u_i(k)) - u_i(k)| < a(k),\ \text{if } |u_i(k)| < a(k). \tag{31}$$

Using (27)–(31) and (6), we obtain

$$\underline{\iota}_{i1} \leq \iota_{i1}(k) \leq \bar{\iota}_{i1}, \iota_{i2}(k) \leq \bar{a}(k), \forall k \geq 0, \tag{32}$$

$$\underline{\iota}_{i1} = \frac{2\underline{\varepsilon}_i}{1 + \underline{\varepsilon}_i}, \bar{\iota}_{i1} = \frac{2}{1 + \underline{\varepsilon}_i}. \tag{33}$$

Substituting (29) into (26) gives us

$$\begin{aligned} s_{i3}(k+1) = (1+\Delta_t\theta_{i3})x_{i3}(k) + \Delta_t g_{i3}(\iota_{i1}(k)u_i(k) + \iota_{i2}(k)) \\ + \Delta_t\textstyle\sum_{j=1}^{n}\delta_{ji}(|x_{i1}|,|x_{i2}|) - z_{i3}(k+1). \end{aligned} \tag{34}$$

Formula (34) can be reorganized into the following form:

$$\begin{aligned} s_{i3}(k+1) = \Delta_t g_{i3}\iota_{i1}(k)[u_i(k) + \tfrac{1}{\Delta_t g_{i3}\iota_{i1}(k)}(\Delta_t g_{i3}\iota_{i2}(k) \\ + (1+\Delta_t\theta_{i3})x_{i3}(k) + \Delta_t\textstyle\sum_{j=1}^{n}\delta_{ji}(|x_{i1}|,|x_{i2}|) \\ - z_{i3}(k+1))]. \end{aligned} \tag{35}$$

Let

$$\begin{aligned} h_{i3}(k) = -\tfrac{1}{\Delta_t g_{i3}\iota_{i1}(k)}[\Delta_t g_{i3}\iota_{i2}(k) + (1+\Delta_t\theta_{i3})x_{i3}(k) \\ + \Delta_t\textstyle\sum_{j=1}^{n}\delta_{ji}(|x_{i1}|,|x_{i2}|) - z_{i3}(k+1)]. \end{aligned} \tag{36}$$

Noting that $h_{i3}(k)$ contains the nonlinear term $\sum_{j=1}^{n}\delta_{ji}(|x_{i1}|,|x_{i2}|)$, $h_{i3}(k)$ can be approximated by RBFNNs

$$h_{i3}(k) = \eta_{i3}^{*T}\psi_{i3}(\xi_{i3}(k)) + \varepsilon_{i3}(\xi_{i3}(k)). \tag{37}$$

Similar to (20), we have $\|\psi_{i3}(\xi_{i3}(k))\|^2 \le l_{i3}$, and $|\varepsilon_{i3}(\xi_{i3}(k))| \le \bar{\varepsilon}_{i3}$,$\xi_{i3}(k) = [\bar{x}_{i3}(k), |x_{i1}|, |x_{i2}|, z_{i3}(k+1)]^T \in \Omega_{\xi_{i3}}$ is the input vector of (37). The control law $u_i(k)$ is designed as

$$u_i(k) = k_{i3}\hat{\eta}_{i3}^T(k)\psi_{i3}(\xi_{i3}(k)), \tag{38}$$

where $k_{i3} > 0$ is a design parameter, and we choose the adaptation law as

$$\hat{\eta}_{i3}(k+1) = \hat{\eta}_{i3}(k) - \lambda_{i3}(\psi_{i3}(\xi_{i3}(k))s_{i3}(k+1) + \sigma_{i3}\hat{\eta}_{i3}(k)), \tag{39}$$

where λ_{i3} and σ_{i3} are the positive design parameters, The term η_{i3}^* can be subtracted from each side of (39), and the following formula is available:

$$\tilde{\eta}_{i3}(k+1) = \tilde{\eta}_{i3}(k) - \lambda_{i3}(\psi_{i3}(\xi_{i3}(k))s_{i3}(k+1) + \sigma_{i3}\hat{\eta}_{i3}(k)). \tag{40}$$

Step 4: Define

$$s_{i4}(k) = y_{i2}(k) - V_{refi}(k) \tag{41}$$

as the fourth error surface; from (9), it yields

$$\begin{aligned} s_{i4}(k+1) =& y_{i2}(k+1) - V_{refi}(k+1) \\ =& x_{i4}(k) + \Delta_t g_{i4}Q(u'_{Bi}(k)) + \Delta_t f_{i4}(\bar{x}_{i4}) \\ & - V_{refi}(k+1). \end{aligned} \tag{42}$$

Similar to (27)–(33), one has:

$$Q(u'_{Bi}(k)) = \iota_{i3}(k)u'_{Bi}(k) + \iota_{i4}(k) \tag{43}$$

where

$$\iota_{i3}(k) = \begin{cases} \frac{Q(u'_{Bi}(k))}{u'_{Bi}(k)}, & \text{if } |u'_{Bi}(k)| \ge a(k), \\ 1, & \text{if } |u'_{Bi}(k)| < a(k), \end{cases} \tag{44}$$

$$\iota_{i4}(k) = \begin{cases} 0, & \text{if } |u'_{Bi}(k)| \ge a(k), \\ Q(u'_{Bi}(k)) - u'_{Bi}(k), & \text{if } |u'_{Bi}(k)| < a(k). \end{cases} \tag{45}$$

By (32) and (45), we have

$$1-\delta \leq \frac{Q(u'_{Bi}(k))}{u'_{Bi}(k)}, \leq 1+\delta, \text{ if } \left|u'_{Bi}(k)\right| \geq a(k), \tag{46}$$

$$\left|Q(u'_{Bi}(k)) - u'_{Bi}(k)\right| < a(k), \text{ if } \left|u'_{Bi}(k)\right| < a(k). \tag{47}$$

From (44)–(47) and (6), we have

$$\underline{\iota}_{i3} \leq \iota_{i3}(k) \leq \bar{\iota}_{i3}, \iota_{i4}(k) \leq \bar{a}(k), \forall k \geq 0, \tag{48}$$

$$\underline{\iota}_{i3} = \frac{2\varepsilon_i}{1+\varepsilon_i}, \bar{\iota}_{i3} = \frac{2}{1+\varepsilon_i}. \tag{49}$$

Then, substituting (43) into (42) gives

$$\begin{aligned} s_{i4}(k+1) = {} & x_{i4}(k) + \Delta_t g_{i4}(\iota_{i3}(k)u'_{Bi}(k) + \iota_{i4}(k)) \\ & + \Delta_t f_{i4}(\bar{x}_{i4}) - V_{refi}(k+1). \end{aligned} \tag{50}$$

Let

$$\begin{aligned} h_{i4}(k) = {} & \frac{1}{\Delta_t g_{i4}\iota_{i3}(k)}(\Delta_t g_{i4}\iota_{i4}(k) + x_{i4}(k) \\ & + \Delta_t f_{i4}(\bar{x}_{i4}) - V_{refi}(k+1)), \end{aligned} \tag{51}$$

then, (50) can be rewritten as

$$s_{i4}(k+1) = \Delta_t g_{i4}\iota_{i3}(k)[u'_{Bi}(k) + h_{i4}(k)]. \tag{52}$$

Similarly, $h_{i4}(k)$ can be approximated by RBFNNs as

$$h_{i4}(k) = \eta_{i4}^{*T}\psi_{i4}(\xi_{i4}(k)) + \varepsilon_{i4}(\xi_{i4}(k)). \tag{53}$$

Similar to (20) and (37), one has $\|\psi_{i4}(\xi_{i4}(k))\|^2 \leq l_{i4}$ and $|\varepsilon_{i4}(\xi_{i4}(k))| \leq \bar{\varepsilon}_{i4}$; the input variable vector of (53) is $\xi_{i4}(k) = [\bar{x}_{i4}(k), V_{refi}(k+1)]^T \in \Omega_{\xi_{i4}}$. Now the final controller $u'_{Bi}(k)$ and adaptive law $\hat{\eta}_{i4}(k)$ are constructed as

$$u'_{Bi}(k) = k_{i4}\hat{\eta}_{i4}^T(k)\psi_{i4}(\xi_{i4}(k)), \tag{54}$$

$$\hat{\eta}_{i4}(k+1) = \hat{\eta}_{i4}(k) - \lambda_{i4}(\psi_{i4}(\xi_{i4}(k))s_{i4}(k+1) + \sigma_{i4}\hat{\eta}_{i4}(k)), \tag{55}$$

where the design parameters $k_{i4} > 0$, $\lambda_{i4} > 0$, and $\sigma_{i4} > 0$.

4. Stability Analysis

The stability analysis for the decentralized discrete adaptive dynamic surface quantized control scheme is presented. Define the filter error of (16) and (24) as

$$\begin{aligned} y_{i2}(k) &= z_{i2}(k) - x_{i2d}(k), \\ y_{i3}(k) &= z_{i3}(k) - x_{i3d}(k), \end{aligned} \tag{56}$$

where $x_{i2d}(k)$, $z_{i2}(k)$, $x_{i3d}(k)$ and $z_{i3}(k)$ are given by (15), (16), (21) and (24). In view of (17) and (25), it follows that

$$\begin{aligned} x_{i2}(k) - x_{i2d}(k) &= s_{i2}(k) + y_{i2}(k), \\ x_{i3}(k) - x_{i3d}(k) &= s_{i3}(k) + y_{i3}(k). \end{aligned} \tag{57}$$

Considering the Lyapunov function candidate

$$V_{i1}(k) = s_{i1}^2(k), \tag{58}$$

then the first forward difference of $V_{i1}(k)$ is computed by

$$\begin{aligned}\Delta V_{i1}(k) &= s_{i1}^2(k+1) - s_{i1}^2(k) \\ &= [x_{i1}(k) + \Delta_t x_{i2}(k) - y_{ri}(k+1)]^2 - s_{i1}^2(k).\end{aligned} \tag{59}$$

$\Delta V_{i1}(k)$ can be rewritten as

$$\begin{aligned}\Delta V_{i1}(k) = [&\Delta_t(x_{i2}(k) - x_{i2d}(k)) + (1-k_{i1})x_{i1}(k) \\ &- (1-k_{i1})y_{ri}(k+1)]^2 - s_{i1}^2(k).\end{aligned} \tag{60}$$

Define the second Lyapunov function candidate as

$$V_{i2}(k) = \tfrac{1}{\Delta_t \bar{g}_{i2}} s_{i2}^2(k) + \tfrac{1}{\lambda_{i2}} \tilde{\eta}_{i2}^T(k)\tilde{\eta}_{i2}(k). \tag{61}$$

The first forward difference of $V_{i2}(k)$ is computed by

$$\begin{aligned}\Delta V_{i2}(k) = &\tfrac{1}{\Delta_t \bar{g}_{i2}} \left[s_{i2}^2(k+1) - s_{i2}^2(k) \right] \\ &+ \tfrac{1}{\lambda_{i2}} \left[\tilde{\eta}_{i2}^T(k+1)\tilde{\eta}_{i2}(k+1) - \tilde{\eta}_{i2}^T(k)\tilde{\eta}_{i2}(k) \right].\end{aligned} \tag{62}$$

Define the third Lyapunov function candidate as

$$V_{i3}(k) = \tfrac{1}{\Delta_t \bar{g}_{i3} \bar{l}_{i1}} s_{i3}^2(k) + \tfrac{1}{\lambda_{i3}} \tilde{\eta}_{i3}^T(k)\tilde{\eta}_{i3}(k). \tag{63}$$

Similar to (60) and (62), we have

$$\begin{aligned}\Delta V_{i3}(k) = &\tfrac{1}{\Delta_t \bar{g}_{i3} \bar{l}_{i1}} \left[s_{i3}^2(k+1) - s_{i3}^2(k) \right] \\ &+ \tfrac{1}{\lambda_{i3}} \left[\tilde{\eta}_{i3}^T(k+1)\tilde{\eta}_{i3}(k+1) - \tilde{\eta}_{i3}^T(k)\tilde{\eta}_{i3}(k) \right].\end{aligned} \tag{64}$$

Then, the Lyapunov function is chosen as

$$V_i(k) = \textstyle\sum_{j=1}^{4} V_{ij}(k) + \sum_{j=2}^{3} y_{ij}^2(k). \tag{65}$$

Therefore, from (56)–(63), we have

$$\Delta V_i(k) = \textstyle\sum_{j=1}^{4} \Delta V_{ij}(k) + \sum_{j=2}^{3} \left[y_{ji}^2(k+1) - y_{ij}^2(k) \right]. \tag{66}$$

Based on the above analysis, the main results are given in Theorem 1.

Theorem 1. *Consider multi-machine power system* (8) *and* (9) *with hysteresis quantizer* (6)*, first-order filters* (16) *and* (24)*, virtual control laws* (15) *and* (21)*, adaptive laws* (22)*,* (39)*, and* (55)*, final controllers* (38) *and* (54)*, and positive definite Lyapunonv function* (65)*. The control system initial values satisfy* $V(0) \leq P, (P > 0)$*; then, by selecting the appropriate sampling time* Δ_t*, and design parameters such as* k_{ij}*,* τ_{ij}*,* λ_{ij}*, and* σ_{ij} *such that all the signals of the closed-loop system are semi-globally uniformly ultimately bounded, and the tracking error will converge to a sufficiently small neighborhood of zero for* $\forall k > 0$*. The details of the proof are given in Appendix A. Regarding stability of the closed-loop system, the closed-loop system structure is shown in Figure 2. Under the designed virtual speed of the generator signals* (T2.2) *and electrical power signals* (T2.5)*, the final controller signals are* (T2.9) *and* (T2.12) *by selecting the appropriate sampling time and design parameters such as* τ_{ij}*,* λ_{ij}*,* σ_{ij} *such that the semi-globally uniformly ultimately boundedness* (*SUUB*) *of all the signals, including the states* $x_{ij}(k), (i = 1, \cdots, n, j = 1, \cdots, 4)$*, the NN weight estimates* $\hat{\eta}_{ij}(i = 1, \cdots, n, j = 2, \cdots, 4)$*, the control input* $u_i(k)$*,* $u'_{Bi}(k)$*, and the tracking errors, converge to a bounded compact set* $\Omega = \{\sum_{i=1}^{n}(s_{i1}(k) + \dfrac{1}{\Delta_t \bar{g}_{i2}} s_{i2}(k) + \dfrac{1}{\Delta_t \bar{g}_{i3} \bar{l}_{i1}} s_{i3}(k) +$

$\frac{1}{\Delta_t \bar{g}_{i4} \bar{\iota}_{i3}} s_{i4}(k) + \sum_{j=2}^{4} \tilde{\eta}_{ij}^{\mathrm{T}}(k)\tilde{\eta}_{ij}(k)/\lambda_{ij} + \sum_{j=2}^{3} y_{ij}^2(k)) \leq P\}$, *with P being a given arbitrarily positive number. The Proof is available in the Appendix A.*

5. Experimental Verification

A two-machine power system model with SVC is used in this experimental process, as shown in Figure 3. The parameters of the system (1) and (A2) are given in Table 2. In order to illustrate the effectiveness of the proposed control scheme, the experiments are completed on the ModelingTech real-time simulation experimental platform of power electronics, which is shown in Figure 4. Figure 5 shows the experimental system architecture.

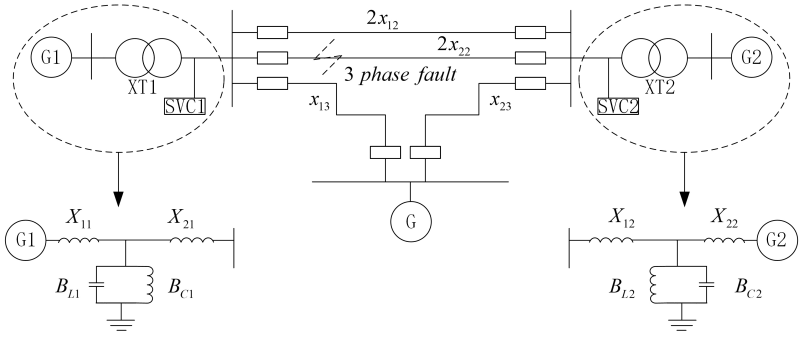

Figure 3. Structure diagram of two-machine excitation system with SVC.

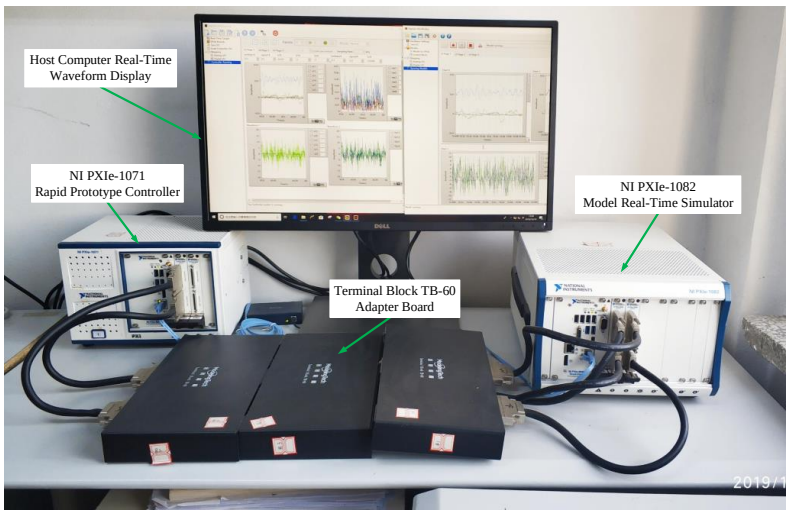

Figure 4. Experimental environment of power electronics.

Table 2. Parameters of the two-machine excitation system with SVC equipment.

Head	*G*#1	Transmission Line	*G*#2
$x_d(p.u.)$	1.863		2.36
$x'_d(p.u.)$	0.257		0.319
$x_T(p.u.)$	0.129		0.11
$x_{ad}(p.u.)$	1.712		1.712
$T'_{d0}(p.u.)$	6.9		7.96
$H(s)$	4		5.1
$D(p.u.)$	5		3
$\omega_0(rad/s)$	314.15		314.12
$x_{12}(p.u.)$		0.55	
$x_{13}(p.u.)$		0.53	
$x_{23}(p.u.)$		0.6	

In these experiments, the operation point is selected as $\delta_{10} = 60.07$ degree, $\omega_{10} = 314.15$ degree/s, $P_{m10} = 1.03$ p.u., $V_{ref1} = 0.96$ p.u., $\delta_{20} = 60.06$ degree, $\omega_{20} = 314.12$ degree/s, $P_{m20} = 1.02$ p.u., and $V_{ref2} = 0.94$ p.u., and we assume that a three-phase short-circuit fault occurs and lasts for 0.2 s at $t = 5.92$ s of the experiment. The control objective is to design the control laws (38) and (54) to achieve the predetermined tracking performance of power angle and access point voltage of SVC. After eliminating the three-phase short-circuit fault, the power angle, speed, and electric power can be kept in a small range near the working point.

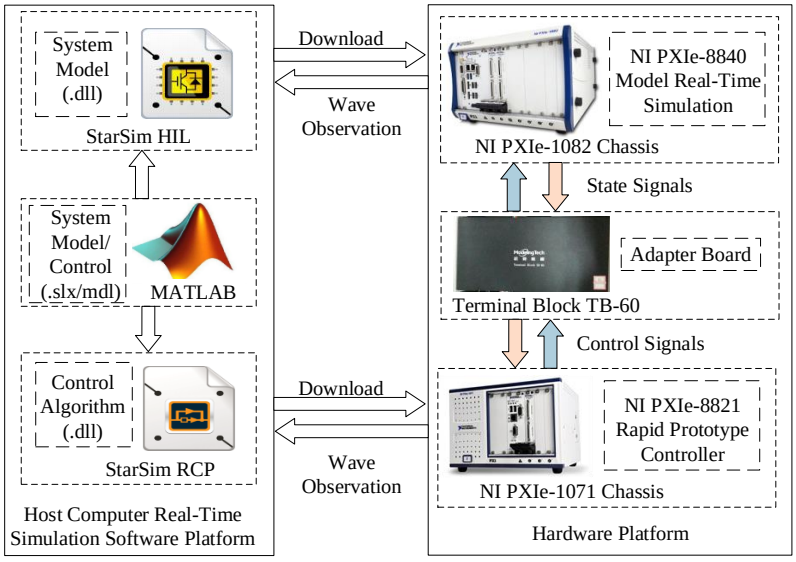

Figure 5. Experimental system architecture.

To achieve the desired tracking error performance, a suitable sampling period Δ_t is a critical issue for a discrete-time control system; in this paper, when considering the model precision, control performance, and computer burden, we choose $\Delta_t = 0.001$ s, $k_{11} = 0.01$, $k_{12} = 0.0014$, $k_{13} = 1.34$, $k_{14} = 1.2$, $k_{112} = 0.215$, $k_{21} = 0.01$, $k_{22} = 0.0015$, $k_{23} = 1.35$, and $k_{24} = 1.3$, $k_{222} = 0.262$. The parameters of the RBFNN regulation law are as follows: $\lambda_{12} = 0.015$, $\sigma_{12} = 0.3$, $\lambda_{13} = 0.07$, $\sigma_{13} = 0.25$, $\lambda_{14} = 0.04$, $\sigma_{14} = 0.6$, $\lambda_{22} = 0.015$, $\sigma_{22} = 0.3$, $\lambda_{23} = 0.08$, $\sigma_{23} = 0.2$, $\lambda_{24} = 0.04$, and $\sigma_{24} = 0.8$. For the RBFNN Gaussian basis function, we select $\psi_{12}(\xi_{12}(k))$ and $\psi_{22}(\xi_{22}(k))$ with 21 nodes and the centers $c_{12l} \in R^3, c_{22l} \in R^3$ evenly spaced in $[-60, +60] \times [-314, +314] \times [-1, +1]$, and width $b_{12l} = b_{22l} = 1, (l = 1, ..., 21)$. For NN Gaussian basis function, we select $\psi_{13}(\xi_{13}(k))$ and $\psi_{23}(\xi_{23}(k))$ with 17 nodes and centers $c_{13l} \in R^4, c_{23l} \in R^4$, evenly spaced in $[-60, +60] \times [-314, +314] \times [-2, +2] \times [-1, +1]$, and width $b_{13l} = b_{23l} = 1, (l = 1, ..., 15)$. For the last RBFNNs Gaussian basis function, we select $\psi_{14}(\xi_{14}(k))$ and $\psi_{24}(\xi_{24}(k))$ with 15 nodes and centers $c_{14l} \in R^5, c_{24l} \in R^5$, evenly spaced in $[-60, +60] \times [-314, +314] \times [-2, +2] \times [-1, +1] \times [-1, +1]$, and width $b_{14l} = b_{24l} = 1, (l = 1, ..., 21)$.

Remark 4. *It is should be noted that the there is no fixed parameter design method for controller parameter selection. It is usually selected according to Equations (A41)–(A47), personal experience, and characteristics of the control system. According to the actual results of the data obtained from the experiment with multiple sets of parameters, we get the optimal solution after repeated comparison and testing.*

Comparison of the proposed control strategy in this paper with traditional discrete-time backstepping (BC) methods are conducted in this experimental. The maximum value of the steady tracking error (MVTE), $E_{\max} = \max|s_{i1}(k)|, k > 8000, i = 1, 2$ and the root mean square values of steady tracking error (RMSVTE), $E_{RMSVTE} = \sqrt{(\sum_{k=m}^{n} s_{i1}(k)/(m-n))}$, $m = 8000, n = 20{,}000, i = 1, 2$, are shown in Table 3.

Remark 5. *According to [48], the control law of the BC method is:*

$$\begin{aligned} u = T_{ci}\{-k_i \sin(x_1+\delta_0)e_2\} - \frac{e_3}{\gamma^2}\left(\frac{c_{2+m_2+\hat{\theta}}}{k_i \sin(x_1+\delta_0)}\right)^2 - c_1 x_2 \\ - \frac{e_3}{2\gamma^2} + \frac{1}{T_{ci}}(x_3 + B_{ci}) - \frac{1}{k_i \sin(x_1+\delta_0)}[c_2 c_1 x_2 + \hat{\theta} x_2 \\ + m_1 x_2 + (c_2 + m_2\hat{\theta})(\hat{\theta} x_2 + a_0 + k_i \sin(x_1+\delta_0)(x_3 \\ + B_{ci}))] + \frac{\cos(x_1+\delta_0)x_2}{k_i \sin^2(x_1+\delta_0)}[m_1 x_1 + m_2 x_2 + \hat{\theta} x_2 + a_0 \\ + c_2 e_2] - \beta e_3\} \end{aligned} \tag{67}$$

$$\dot{\hat{\theta}} = \rho[e_2 + \frac{e_3(c_2 + m_2 + \hat{\theta})}{k_i \sin(x_1+\delta_0)}]x_2 \tag{68}$$

with $k_i = \omega_{i0}/E'_{qi}H_iD_i, m_1 = c_1/\gamma^2 - 1/2c_1q_2^2 + \sigma, m_2 = 1/\gamma^2 + 1/2q_2^2 + c_1, m_3 = \varepsilon_1/\gamma^2 - 1/2q_2^2\varepsilon_1 + \varepsilon_1$. *The parameters of the BC control method are:* $c_1 = c_2 = 2.6, \rho = 1, \beta = 95, \gamma = 1, \varepsilon_1 = \varepsilon_2 = 25, \sigma = 30, q_1 = q_2 = 0.45$; *otherwise,* $\delta_0, \omega_{i0}, T_{ci}, B_{ci}, E'_{qi}, H_i, D_i$ *are same as the original version.*

Table 3. The MVTE of the power angle.

Type of Error (Degree)		MVTE	RMSVTE
Backstepping	*G*#1	0.0277	0.0164
Scheme	*G*#2	0.0501	0.0157
Proposed	*G*#1	0.0150	0.0066
Scheme	*G*#2	0.0118	0.0036

Remark 6. *In Figure 6, to be more consistent with the actual situation, the initial speed parameters of the two machines in this paper are different, so there will be phase offset in the two machines. When the three-phase short circuit is triggered, if the two motors are not in the same phase, there will be different results.*

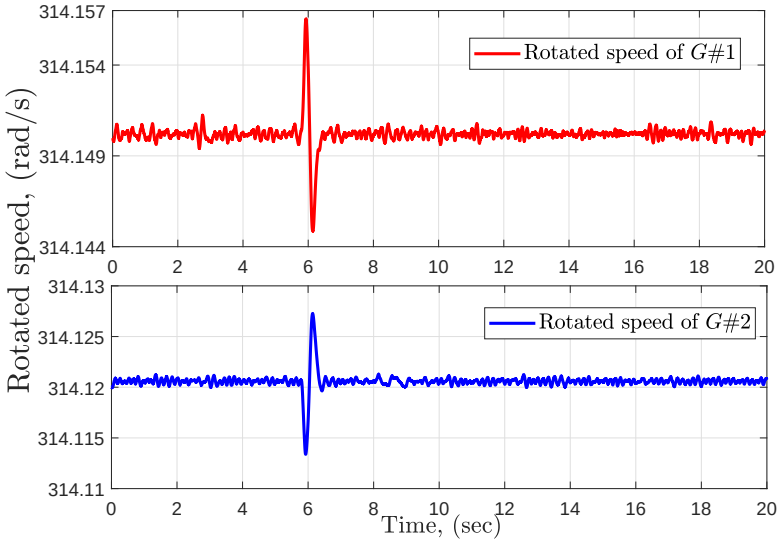

Figure 6. Response curves of rotated speed.

The results of the experiment are shown in Figures 7–14. Figure 7 shows the power angle output error performance comparison of the two control strategies. It can be seen that under the actions of the proposed controller (38) and (54), there is smaller steady output error and better transient response performance. Figure 8 presents response curves of the power angles by using the proposed control algorithm. Figures 6–12, respectively, introduce the rotating speed, electric power, control signals, access point voltage of SVC, and the control input of SVC for $G\#1$ and $G\#2$. Figures 13 and 14 show weight-norm estimation of the RBFNNs.

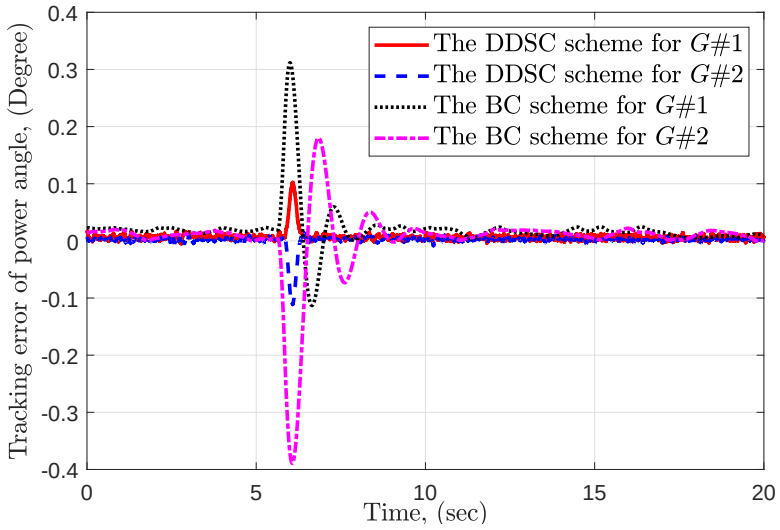

Figure 7. Tracking error of power angle.

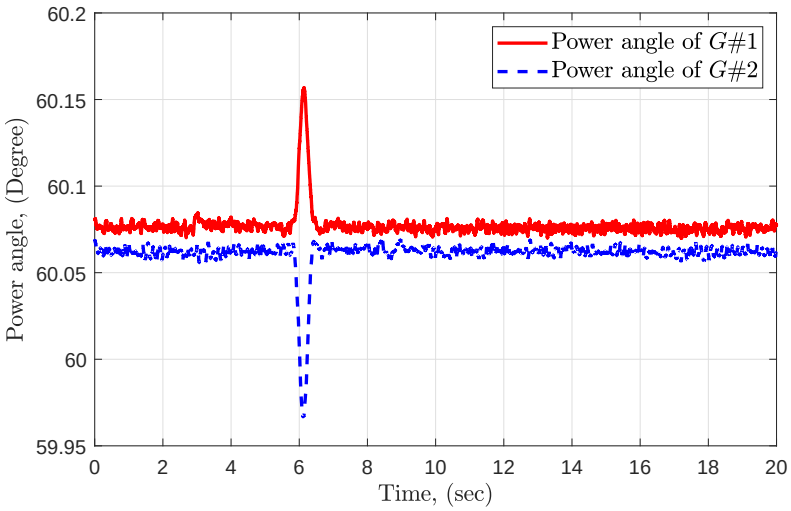

Figure 8. Tracking performance of power angle.

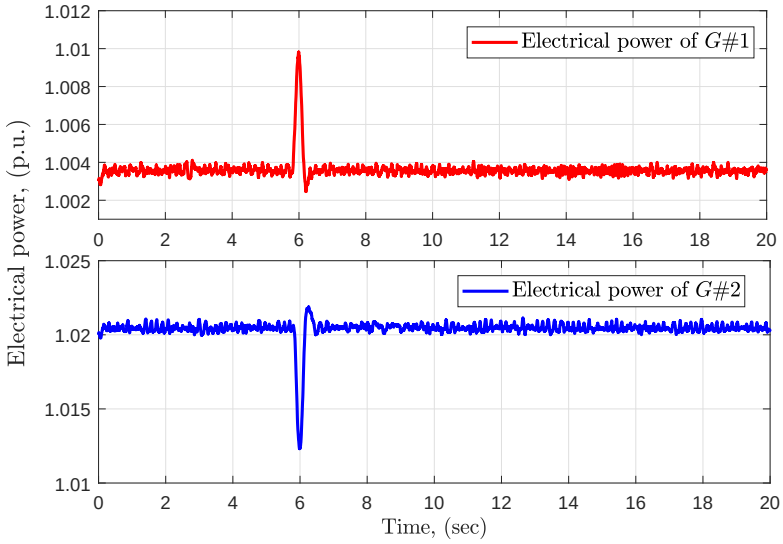

Figure 9. Response curves of electrical power *Pe*.

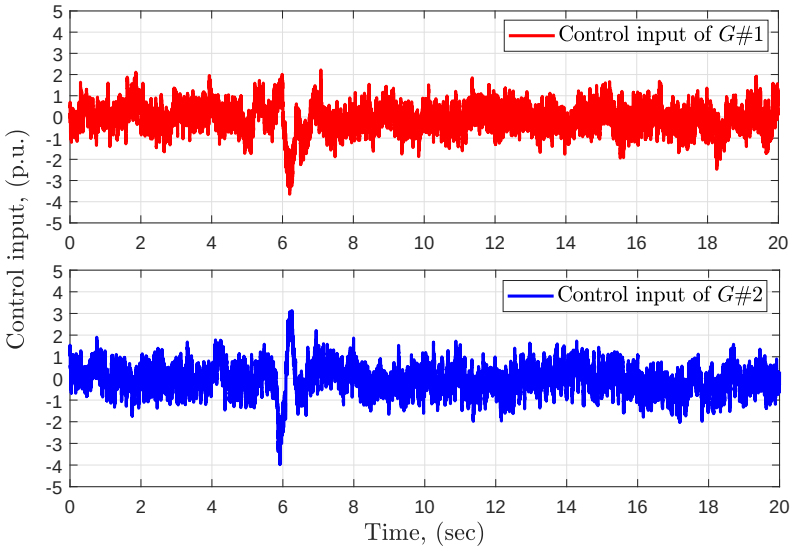

Figure 10. Control input of Generator 1.

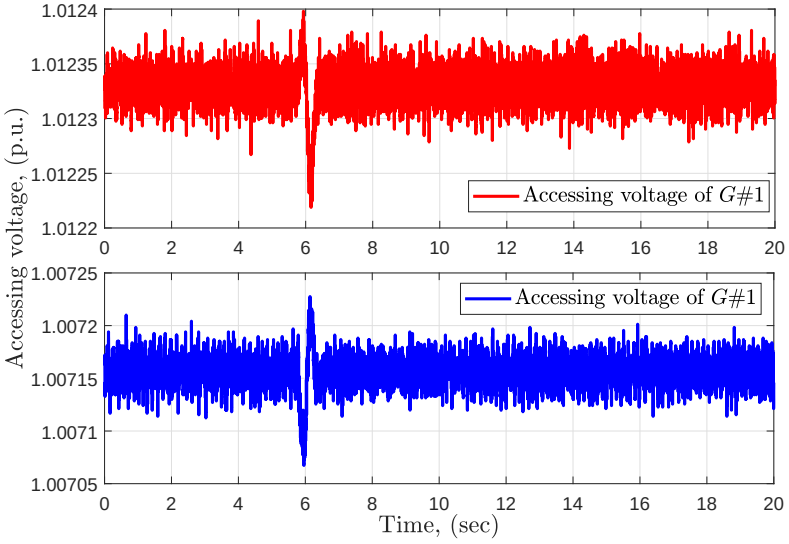

Figure 11. Accessing voltage of SVC.

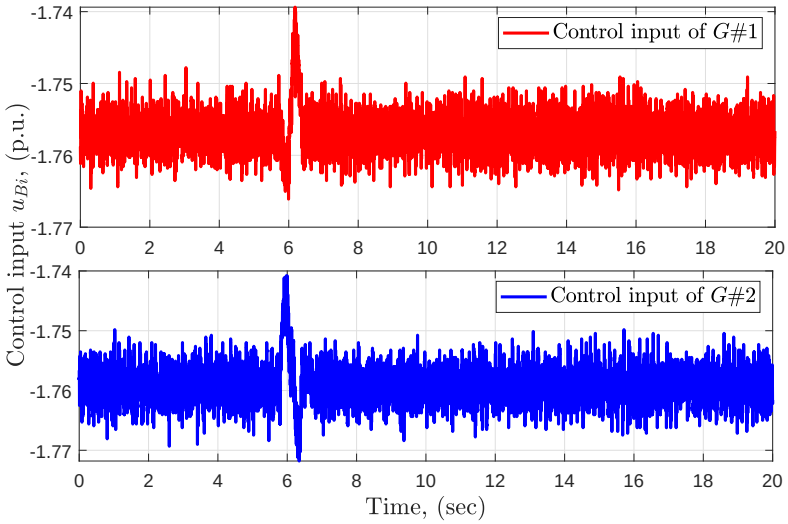

Figure 12. Control input of SVC Generator 1.

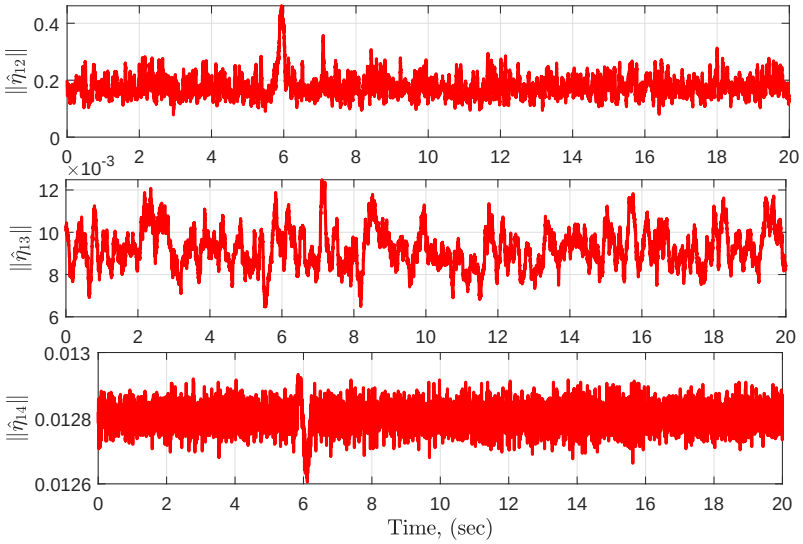

Figure 13. Weight-norm estimation of RBFNNs.

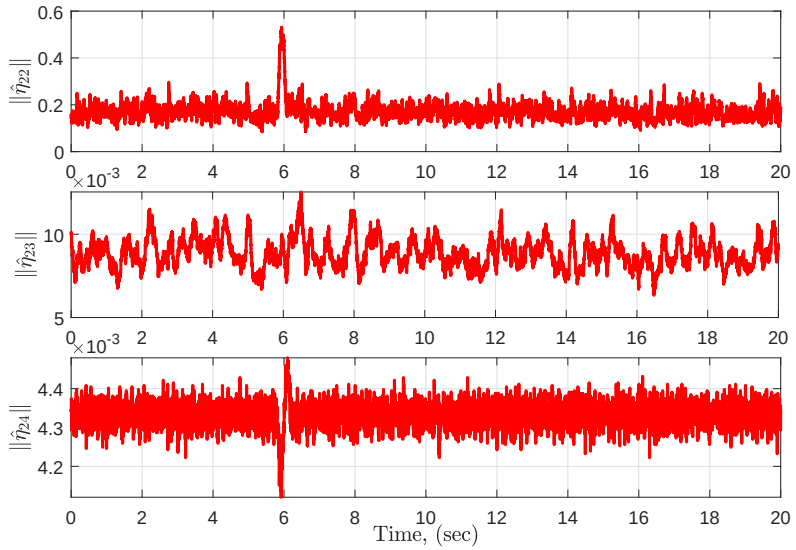

Figure 14. Weight-norm estimation of RBFNNs for Generator 2.

6. Results and Discussions

In this article, a discrete-time adaptive decentralized control scheme is developed to deal with the stability of multi-machine power systems. An external disturbance and subsystem interconnection are considered. By utilizing a digital first-order low-pass filter, the adaptation laws and controller are designed based on discrete-time control theory, and the non-causal problems that lead to the complex structure of the controller are effectively avoided. The improved hysteresis quantizer realizes quantization of amplitude of the control input signal while discretizing in time, which can improve the stability of the power system and reduce the chattering phenomena, so a digital adaptive controller of the multi-machine power system is designed. Stability analysis based on Lyapunov's method shows that all signals of the whole closed-loop system are SUUB, and the proposed control algorithm is verified through the ModelingTech real-time experiment platform of power electronics, which shows that the control strategy achieves the expected control effect. The proposed method provides 0.0127 and 0.0383 less MVTE, as well as 0.0098 and 0.0121 less RMSVTE compared to BC in G#1 and G#2, respectively.

Author Contributions: Conceptualization, G.C. and X.Z.; methodology, J.Z.; software, M.W. and P.L.; validation, P.L., J.G., and M.W.; formal analysis, J.G. and M.W.; investigation, J.G. and M.W.; data curation, J.G. and M.W.; writing—original draft preparation, J.G., P.L., and M.W.; writing—review and editing, X.Z.; visualization, J.G. and M.W.; supervision, G.C., X.Z., and H.H.; project administration, G.C. and X.Z.; funding acquisition, G.C. and X.Z. All authors have read and agreed to the published version of the manuscript.

Funding: This research was funded by the Science and Technology Project of Jilin Province, grant number 20210509053RQ.

Institutional Review Board Statement: Not applicable.

Informed Consent Statement: Not applicable.

Data Availability Statement: Not applicable.

Conflicts of Interest: The authors declare no conflict of interest.

Appendix A

Appendix A.1. Problem Statement

From (1), the electrical equations are:

$$\begin{cases} E_{fi}(t) = k_{ei}u_{fi}, \\ I_{qi}(t) = \sum_{j=1}^{n} E'_{qj}(t)B_{ij}\sin(\delta_i - \delta_j), \\ E_{qi}(t) = x_{adi}I_{fi}(t) = E'_{qi}(t) + (x_{di} - x'_{di})I_{di}(t), \\ I_{di}(t) = -\sum_{j=1}^{n} E'_{qj}(t)B_{ij}\cos(\delta_i - \delta_j), \\ P_{ei}(t) = \sum_{j=1}^{n} E'_{qi}(t)E'_{qj}(t)B_{ij}\sin(\delta_i - \delta_j), \\ Q_{ei}(t) = -\sum_{j=1}^{n} E'_{qi}(t)E'_{qj}(t)B_{ij}\cos(\delta_i - \delta_j). \end{cases} \tag{A1}$$

According to [49,50], the SVC model is expressed as:

$$\dot{B}_{Li} = \frac{1}{T_{ci}}(-B_{Li} + B_{Ci} + u_{Bi}), \tag{A2}$$

where i represents the ith generator of n-interconnected generators, d_i is a composite disturbance signal that includes continuous changes in input mechanical power and load, unknown system interference, etc.

According to [4], defining $P_{mi} = P_{mi0}$ as a positive constant, the dynamic model (1), (A1), and (A2) can be transformed into the following form:

$$\begin{aligned}\dot{\delta}_i(t) &= \omega_i,\\ \dot{\omega}_i(t) &= -\tfrac{D_i}{2H_i}\omega_i(t) - \tfrac{\omega_0}{2H_i}\Delta P_{ei} + d_i,\\ \Delta\dot{P}_{ei}(t) &= -\tfrac{1}{T'_{d0i}}\Delta P_{ei}(t) + \tfrac{1}{T'_{d0i}}u_i + \gamma_i(\delta,\omega).\end{aligned} \tag{A3}$$

where u_i and $\gamma_i(\delta,\omega)$ represent the control input and interconnection items, respectively, and can be expressed as

$$u_i = I_{qi}E_{fi} - (x_{di} - x'_{di})I_{di}I_{qi} - P_{mi} - T'_{d0i}Q_{ei}\omega_i \tag{A4}$$

$$\gamma_i(\delta,\omega) = E'_{qi}\sum_{j=1}^{n}\dot{E}'_{qj}(t)B_{ij}\sin(\delta_i-\delta_j) - E'_{qi}\sum_{j=1}^{n}E'_{qj}(t)B_{ij}\cos(\delta_i-\delta_j)\omega_j, \tag{A5}$$

and $\gamma_i(\delta,\omega)$ satisfies

$$|\gamma_i(\delta,\omega)| \le \textstyle\sum_{j=1}^{n}(\gamma_{i1j}|\delta_j| + \gamma_{i2}|\omega_j|), \tag{A6}$$

where $\gamma_{i1j} = \sum_{j=1,j\neq i}^{n}\frac{4P_{1ij}}{|T'_{d0j}|_{\min}}|P_{ei}|_{\max}$, when $j = i$ or $\gamma_{i1j} = \frac{4P_{1ij}}{|T'_{d0j}|_{\min}}|P_{ei}|_{\max}$, when $j \neq i$, $\gamma_{i2} = P_{2ij}|Q_{ei}|_{\max}$, with P_{1ij} and P_{2ij} being either 1 or 0, and $(\bullet)_{min}$ and $(\bullet)_{max}$ represent the minimum and maximum values of $(\bullet)$. Then, the last two equations in (A1) can be rewritten as:

$$P_{ei} = E'_{qi}I_{qi}, Q_{ei} = E'_{qi}I_{di}. \tag{A7}$$

Let the ith system state vector $\bar{x}_{i4} = [x_{i1}, x_{i2}, x_{i3}, x_{i4}]^T = [\delta_i, \omega_i, \Delta P_{ei}, \Delta V_{mi}]^T$, where $\Delta P_{ei} = P_{ei} - P_{mi}$, $\Delta V_{mi} = V_{mi} - V_{refi}$ with

$$V_{mi} = \frac{\sqrt{(X_{2i}E'_{qi})^2 + (X_{1i})^2 + 2X_{1i}X_{2i}E'_{qi}\cos x_{i1}}}{X'_{d\Sigma i}}, \tag{A8}$$

where $X_{1i} = x'_{di} + X_{Ti}$, $X'_{d\Sigma i} = X_{1i} + X_{2i} + X_{1i}X_{2i}(B_{Li} - B_{Ci})$, with X_{2i} and X_{Ti} the reactance of the transmission line and the transformer, respectively. Then, (A3) and (A2) can be converted into (2) and (3).

Appendix A.2. Proof of Theorem 1

Substituting (57) into (60) gives us

$$\begin{aligned}\Delta V_{i1}(k) &= [\Delta_t(s_{i2}(k) + y_{i2}(k)) + (1-k_{i1})x_{i1}(k)\\ &\quad - (1-k_{i1})y_{ri}(k+1)]^2 - s_{i1}^2(k),\\ &= [\Delta_t(s_{i2}(k) + y_{i2}(k)) + B_{1i}(\cdot)]^2 - s_{i1}^2(k),\end{aligned} \tag{A9}$$

where $B_{1i}(\cdot) = (1-k_{i1})x_{i1}(k) - (1-k_{i1})y_{ri}(k+1)$. Then, according to Young's inequality, (A9) can be rewritten as

$$\Delta V_{i1}(k) \le 3\Delta_t^2 s_{i2}^2(k) + 3\Delta_t^2 y_{i2}^2(k) + 3B_{1i}^2 - s_{i1}^2(k). \tag{A10}$$

Substituting (23) into (62) can yield

$$\begin{aligned}\Delta V_{i2}(k) = & \tfrac{1}{\Delta_t \bar{g}_{i2}}\left[s_{i2}^2(k+1) - s_{i2}^2(k)\right] \\ & - 2\tilde{\eta}_{i2}^T(k)\psi_{i2}(\xi_{i2}(k))s_{i2}(k+1) - 2\sigma_{i2}\tilde{\eta}_{i2}^T(k)\hat{\eta}_{i2}(k) \\ & + \lambda_{i2}\psi_{i2}^T(\xi_{i2}(k))\psi_{i2}(\xi_{i2}(k))s_{i2}^2(k+1) \\ & + 2\lambda_{i2}\sigma_{i2}\hat{\eta}_{i2}^T(k)\psi_{i2}(\xi_{i2}(k))s_{i2}(k+1) \\ & + \lambda_{i2}\sigma_{i2}^2\hat{\eta}_{i2}^T(k)\hat{\eta}_{i2}(k), \end{aligned} \tag{A11}$$

where

$$\begin{aligned} & - 2\sigma_{i2}\tilde{\eta}_{i2}^T(k)\hat{\eta}_{i2}(k) \\ & = -\sigma_{i2}\|\tilde{\eta}_{i2}(k)\|^2 - \sigma_{i2}\|\hat{\eta}_{i2}(k)\|^2 + \sigma_{i2}\|\eta_{i2}^*(k)\|^2. \end{aligned} \tag{A12}$$

From (18)–(20) and (21), we can obtain

$$\begin{aligned} & \tilde{\eta}_{i2}^T(k)\psi_{i2}(\xi_{i2}(k)) = \tfrac{s_{i2}(k+1)}{\Delta_t g_{i2}} + (s_{i3}(k) + y_{i3}(k)) + \varepsilon_{i2}(\xi_{i2}(k)) \\ & + k_{ii2}s_{i2}(k) + (1+k_{i2})\hat{\eta}_{i2}^{\mathrm{T}}(k)\psi_{i2}(\xi_{i2}(k)) \end{aligned} \tag{A13}$$

$$\begin{aligned} & - 2\tilde{\eta}_{i2}^T(k)\psi_{i2}(\xi_{i2}(k))s_{i2}(k+1) \\ & = -2\tfrac{s_{i2}^2(k+1)}{\Delta_t g_{i2}} - 2\varepsilon_{i2}(\xi_{i2}(k))s_{i2}(k+1) - 2s_{i3}(k)s_{i2}(k+1) \\ & - 2y_{i3}(k)s_{i2}(k+1) - 2k_{ii2}s_{i2}(k)s_{i2}(k+1) \\ & - 2(1+k_{i2})\hat{\eta}_{i2}^T(k)\psi_{i2}(\xi_{i2}(k))s_{i2}(k+1). \end{aligned} \tag{A14}$$

By Young's inequality and $|\varepsilon_{i2}(\xi_{i2}(k))| \le \bar{\varepsilon}_{i2}$, we have

$$-2\varepsilon_{i2}(\xi_{i2}(k))s_{i2}(k+1) \le \tfrac{\Delta_t \bar{g}_{i2}}{\lambda_{i2}}\bar{\varepsilon}_{i2}^2 + \tfrac{\lambda_{i2}}{\Delta_t \bar{g}_{i2}}s_{i2}^2(k+1), \tag{A15}$$

$$-2s_{i3}(k)s_{i2}(k+1) \le \tfrac{\Delta_t \bar{g}_{i2}}{\lambda_{i2}}s_{i3}^2(k) + \tfrac{\lambda_{i2}}{\Delta_t \bar{g}_{i2}}s_{i2}^2(k+1), \tag{A16}$$

$$-2y_{i3}(k)s_{i2}(k+1) \le \frac{1}{2}y_{i3}^2(k) + 2s_{i2}^2(k+1), \tag{A17}$$

$$-2k_{ii2}s_{i2}(k)s_{i2}(k+1) \le \tfrac{\Delta_t \bar{g}_{i2}k_{ii2}^2}{\lambda_{i2}}s_{i2}^2(k) + \tfrac{\lambda_{i2}}{\Delta_t \bar{g}_{i2}}s_{i2}^2(k+1). \tag{A18}$$

Similarly, we have

$$\lambda_{i2}\psi_{i2}^T(\xi_{i2}(k))\psi_{i2}(\xi_{i2}(k))s_{i2}^2(k+1) \le \lambda_{i2}l_{i2}s_{i2}^2(k+1), \tag{A19}$$

$$\begin{aligned} & 2\lambda_{i2}\sigma_{i2}\hat{\eta}_{i2}^T(k)\psi_{i2}(\xi_{i2}(k))s_{i2}(k+1) \\ & \le \tfrac{\lambda_{i2}l_{i2}}{\Delta_t \bar{g}_{i2}}s_{i2}^2(k+1) + \Delta_t \bar{g}_{i2}\lambda_{i2}\sigma_{i2}^2\|\hat{\eta}_{i2}(k)\|^2, \end{aligned} \tag{A20}$$

$$\begin{aligned} & - 2(1+k_{i2})\hat{\eta}_{i2}^T(k)\psi_{i2}(\xi_{i2}(k))s_{i2}(k+1) \\ & \le 2l_{i2}s_{i2}^2(k+1) + \tfrac{1}{2}(1+k_{i2})^2\|\hat{\eta}_{i2}(k)\|^2, \end{aligned} \tag{A21}$$

$$\lambda_{i2}\sigma_{i2}^2\hat{\eta}_{i2}^T(k)\hat{\eta}_{i2}(k) \le \lambda_{i2}\sigma_{i2}^2\|\hat{\eta}_{i2}(k)\|^2. \tag{A22}$$

Substituting (A12)–(A22) into (A11) yields

$$\begin{aligned}
&\Delta V_{i2}(k)\\
&\leq [-\tfrac{1}{\Delta_t \bar{g}_{i2}} + \lambda_{i2} l_{i2} + 2l_{i2} + 2 + \tfrac{\lambda_{i2} l_{i2}}{\Delta_t \bar{g}_{i2}} + 3\tfrac{\lambda_{i2}}{\Delta_t \bar{g}_{i2}}] s_{i2}^2(k+1)\\
&+ [\tfrac{\Delta_t \bar{g}_{i2} k_{ii2}^2}{\lambda_{i2}} - \tfrac{1}{\Delta_t \bar{g}_{i2}}] s_{i2}^2(k) + [\sigma_{i2}(\lambda_{i2}\sigma_{i2} + \Delta_t \bar{g}_{i2}\lambda_{i2}\sigma_{i2} - 1)\\
&+ \tfrac{(1+k_{i2})^2}{2}] \|\hat{\eta}_{i2}(k)\|^2 - \sigma_{i2}\|\tilde{\eta}_{i2}(k)\|^2 + \sigma_{i2}\|\eta_{i2}^*(k)\|^2\\
&+ \tfrac{\Delta_t \bar{g}_{i2}}{\lambda_{i2}} \bar{\varepsilon}_{i2}^2 + \tfrac{\Delta_t \bar{g}_{i2}}{\lambda_{i2}} s_{i3}^2(k) + \tfrac{1}{2} y_{i3}^2(k).
\end{aligned} \tag{A23}$$

Substituting (40) into (64) can yield

$$\begin{aligned}
&\Delta V_{i3}(k)\\
&= \tfrac{1}{\Delta_t \bar{g}_{i3} \bar{\iota}_{i1}} \left[s_{i3}^2(k+1) - s_{i3}^2(k) \right] - 2\tilde{\eta}_{i3}^T(k) \psi_{i3}(\xi_{i3}(k)) s_{i3}(k+1)\\
&- 2\sigma_{i3} \tilde{\eta}_{i3}^T(k) \hat{\eta}_{i3}(k) + \lambda_{i3} \psi_{i3}^T(\xi_{i3}(k)) \psi_{i3}(\xi_{i3}(k)) s_{i3}^2(k+1)\\
&+ 2\lambda_{i3}\sigma_{i3} \hat{\eta}_{i3}^T(k) \psi_{i3}(\xi_{i3}(k)) s_{i3}(k+1)\\
&+ \lambda_{i3}\sigma_{i3}^2 \hat{\eta}_{i3}^T(k) \hat{\eta}_{i3}(k),
\end{aligned} \tag{A24}$$

where

$$\begin{aligned}
&-2\sigma_{i3} \tilde{\eta}_{i3}^T(k) \hat{\eta}_{i3}(k)\\
&= -\sigma_{i3}\|\tilde{\eta}_{i3}(k)\|^2 - \sigma_{i3}\|\hat{\eta}_{i3}(k)\|^2 + \sigma_{i3}\|\eta_{i3}^*(k)\|^2.
\end{aligned} \tag{A25}$$

From (35)–(37) and (T2.9), we can obtain

$$\begin{aligned}
\tilde{\eta}_{i3}^T(k) \psi_{i3}(\xi_{i3}(k)) &= \tfrac{s_{i3}(k+1)}{\Delta_t g_{i3} \iota_{i1}(k)} + \varepsilon_{i3}(\xi_{i3}(k))\\
&+ (1 - k_{i3}) \hat{\eta}_{i3}^T(k) \psi_{i3}(\xi_{i3}(k))
\end{aligned} \tag{A26}$$

$$\begin{aligned}
&-2\tilde{\eta}_{i3}^T(k) \psi_{i3}(\xi_{i3}(k)) s_{i3}(k+1)\\
&= -\tfrac{2}{\Delta_t g_{i3} \iota_{i1}(k)} s_{i3}^2(k+1) - 2\varepsilon_{i3}(\xi_{i3}(k)) s_{i3}(k+1)\\
&- 2(1 - k_{i3}) \hat{\eta}_{i3}^T(k) \psi_{i3}(\xi_{i3}(k)) s_{i3}(k+1).
\end{aligned} \tag{A27}$$

Then, according to Young's inequality and $|\varepsilon_{i3}(\xi_{i3}(k))| \leq \bar{\varepsilon}_{i3}$, we have

$$-2\varepsilon_{i3}(\xi_{i3}(k)) s_{i3}(k+1) \leq \tfrac{\Delta_t \bar{g}_{i3} \bar{\iota}_{i1}}{\lambda_{i3}} \bar{\varepsilon}_{i3}^2 + \tfrac{\lambda_{i3}}{\Delta_t \bar{g}_{i3} \bar{\iota}_{i1}} s_{i3}^2(k+1). \tag{A28}$$

According to Young's inequality and $\|\psi_{i3}(\xi_{i3}(k))\|^2 \leq l_{i3}$, we have

$$\lambda_{i3} \psi_{i3}^T(\xi_{i3}(k)) \psi_{i3}(\xi_{i3}(k)) s_{i3}^2(k+1) \leq \lambda_{i3} l_{i3} s_{i3}^2(k+1), \tag{A29}$$

$$\begin{aligned}
&2\lambda_{i3}\sigma_{i3} \hat{\eta}_{i3}^T(k) \psi_{i3}(\xi_{i3}(k)) s_{i3}(k+1)\\
&\leq \tfrac{\lambda_{i3} l_{i3}}{\Delta_t \bar{g}_{i3} \bar{\iota}_{i1}} s_{i3}^2(k+1) + \Delta_t \bar{g}_{i3} \bar{\iota}_{i1} \lambda_{i3} \sigma_{i3}^2 \|\hat{\eta}_{i3}(k)\|^2,
\end{aligned} \tag{A30}$$

$$\begin{aligned}
&-2(1 - k_{i3}) \hat{\eta}_{i3}^T(k) \psi_{i3}(\xi_{i3}(k)) s_{i3}(k+1)\\
&\leq l_{i3} s_{i3}^2(k+1) + (1 - k_{i3})^2 \|\hat{\eta}_{i3}(k)\|^2,
\end{aligned} \tag{A31}$$

$$\lambda_{i3}\sigma_{i3}^2 \hat{\eta}_{i3}^T(k) \hat{\eta}_{i3}(k) \leq \lambda_{i3}\sigma_{i3}^2 \|\hat{\eta}_{i3}(k)\|^2. \tag{A32}$$

Substituting (A25)–(A32) into (A24) can obtain

$$\begin{aligned}
&\Delta V_{i3}(k)\\
&\leq [-\tfrac{1}{\Delta_t \bar{g}_{i3}\bar{l}_{i1}} + \lambda_{i3}l_{i3} + l_{i3} + \tfrac{\lambda_{i3}l_{i3}}{\Delta_t \bar{g}_{i3}\bar{l}_{i1}} + \tfrac{\lambda_{i3}}{\Delta_t \bar{g}_{i3}\bar{l}_{i1}}]s_{i3}^2(k+1)\\
&- \tfrac{1}{\Delta_t \bar{g}_{i3}\bar{l}_{i1}}s_{i3}^2(k) + \tfrac{\Delta_t \bar{g}_{i3}\bar{l}_{i1}}{\lambda_{i3}}\bar{\varepsilon}_{i3}^2 - \sigma_{i3}\|\tilde{\eta}_{i3}(k)\|^2 + \sigma_{i3}\|\eta_{i3}^*(k)\|^2\\
&+ [\sigma_{i3}(\lambda_{i3}\sigma_{i3} + \Delta_t \bar{g}_{i3}\bar{l}_{i1}\lambda_{i3}\sigma_{i3} - 1) + (1-k_{i3})^2]\|\hat{\eta}_{i3}(k)\|^2.
\end{aligned} \tag{A33}$$

Similarly, we obtain

$$\begin{aligned}
&\Delta V_{i4}(k)\\
&\leq \left[-\tfrac{1}{\Delta_t \bar{g}_{i4}\bar{l}_{i3}} + \lambda_{i4}l_{i4} + l_{i4} + \tfrac{\lambda_{i4}l_{i4}}{\Delta_t \bar{g}_{i4}\bar{l}_{i3}} + \tfrac{\lambda_{i4}}{\Delta_t \bar{g}_{i4}\bar{l}_{i3}(k)}\right]s_{i4}^2(k+1)\\
&- \tfrac{1}{\Delta_t \bar{g}_{i4}\bar{l}_{i3}(k)}s_{i4}^2(k) + \tfrac{\Delta_t \bar{g}_{i4}\bar{l}_{i3}}{\lambda_{i4}}\bar{\varepsilon}_{i4}^2 - \sigma_{i4}\|\tilde{\eta}_{i4}(k)\|^2 + \sigma_{i4}\|\eta_{i4}^*(k)\|^2\\
&+ \left[\sigma_{i4}(\lambda_{i4}\sigma_{i4} + \Delta_t \bar{g}_{i4}\bar{l}_{i3}\lambda_{i4}\sigma_{i4} - 1) + (1-k_{i4})^2\right]\|\hat{\eta}_{i4}(k)\|^2.
\end{aligned} \tag{A34}$$

On the basis of (15), (16), and (56), we have

$$\begin{aligned}
y_{i2}^2(k+1) - y_{i2}^2(k) &= [z_{i2}(k+1) - x_{i2d}(k+1)]^2 - y_{i2}^2(k)\\
&= \left[\tfrac{-b_{i2}y_{i2}(k)}{\tau_{i2}} + B_{2i}(\cdot)\right]^2 - y_{i2}^2(k)\\
&= \tfrac{b_{i2}^2 y_{i2}^2(k)}{\tau_{i2}^2} - 2\tfrac{b_{i2}y_{i2}(k)}{\tau_{i2}}B_{2i} + B_{2i}^2 - y_{i2}^2(k).
\end{aligned} \tag{A35}$$

where $B_{2i}(\cdot) = \frac{(1-b_{i2})x_{i2d}(k)}{\tau_{i2}} - \frac{k_{i1}}{\Delta_t}[-x_{i1}(k+1) + y_{ri}(k+2)]$. By Young's inequality, we have

$$-2\tfrac{b_{i2}y_{i2}(k)}{\tau_{i2}}B_{2i} \leq \tfrac{1}{v_{2i}}\tfrac{b_{i2}^2 y_{i2}^2(k)}{\tau_{i2}^2} + v_{2i}B_{2i}^2, \tag{A36}$$

where $v_{2i} > 0$ is a design parameter. Then, (A35) can be rewritten as

$$y_{i2}^2(k+1) - y_{i2}^2(k) \leq \left(\tfrac{v_{2i}b_{i2}^2 + b_{i2}^2}{v_{2i}\tau_{i2}^2} - 1\right)y_{i2}^2(k) + (v_{2i}+1)B_{2i}^2. \tag{A37}$$

Similarly,

$$y_{i3}^2(k+1) - y_{i3}^2(k) \leq \left(\tfrac{v_{3i}b_{i3}^2 + b_{i3}^2}{v_{3i}\tau_{i3}^2} - 1\right)y_{i3}^2(k) + (v_{3i}+1)B_{3i}^2. \tag{A38}$$

Note that Ω_r is compact due to the definition of compact sets Ω_r in Theorem 1. Therefore, $|B_{1i}|, |B_{2i}|, |B_{3i}| (i = 1, ..., n)$ have the maximum values M_{1i}, M_{2i}, M_{3i} on the compact $\Omega_r \times \Omega$. Substituting (A10), (A23), (A33), (A34), (A37), and (A38) into (66), we obtain

$$\begin{aligned}
&\Delta V_i(k) \leq -s_{i1}^2(k) - (\tfrac{1}{\Delta_t \bar{g}_{i2}} - 3\Delta_t^2 - \tfrac{\Delta_t \bar{g}_{i2}k_{ii2}^2}{\lambda_{i2}})s_{i2}^2(k)\\
&- (\tfrac{1}{\Delta_t \bar{g}_{i3}\bar{l}_{i1}} - \tfrac{\Delta_t \bar{g}_{i2}}{\lambda_{i2}})s_{i3}^2(k) - \tfrac{1}{\Delta_t \bar{g}_{i4}\bar{l}_{i3}}s_{i4}^2(k)\\
&+ (\tfrac{v_{2i}b_{i2}^2 + b_{i2}^2}{v_{2i}\tau_{i2}^2} - 1 + 3\Delta_t^2)y_{i2}^2(k) + (\tfrac{v_{3i}b_{i3}^2 + b_{i3}^2}{v_{3i}\tau_{i3}^2} - \tfrac{1}{2})y_{i3}^2(k)
\end{aligned}$$

$$
\begin{aligned}
&+\left[-\tfrac{1}{\Delta_t\bar{g}_{i2}}+\lambda_{i2}l_{i2}+2l_{i2}+2+\tfrac{\lambda_{i2}l_{i2}}{\Delta_t\bar{g}_{i2}}+3\tfrac{\lambda_{i2}}{\Delta_t\bar{g}_{i2}}\right]s_{i2}^2(k+1)\\
&+\left[\sigma_{i2}(\lambda_{i2}\sigma_{i2}+\Delta_t\bar{g}_{i2}\lambda_{i2}\sigma_{i2}-1)+(1+k_{i2})^2/2\right]\|\hat{\eta}_{i2}(k)\|^2\\
&+\left[-\tfrac{1}{\Delta_t\bar{g}_{i3}\bar{\iota}_{i1}}+\lambda_{i3}l_{i3}+l_{i3}+\tfrac{\lambda_{i3}l_{i3}}{\Delta_t\bar{g}_{i3}\bar{\iota}_{i1}}+\tfrac{\lambda_{i3}}{\Delta_t\bar{g}_{i3}\bar{\iota}_{i1}}\right]s_{i3}^2(k+1)\\
&+\left[\sigma_{i3}(\lambda_{i3}\sigma_{i3}+\Delta_t\bar{g}_{i3}\bar{\iota}_{i1}\lambda_{i3}\sigma_{i3}-1)+(1-k_{i3})^2\right]\|\hat{\eta}_{i3}(k)\|^2\\
&+\left[-\tfrac{1}{\Delta_t\bar{g}_{i4}\bar{\iota}_{i3}}+\lambda_{i4}l_{i4}+l_{i4}+\tfrac{\lambda_{i4}l_{i4}}{\Delta_t\bar{g}_{i4}\bar{\iota}_{i3}}+\tfrac{\lambda_{i4}}{\Delta_t\bar{g}_{i4}\bar{\iota}_{i3}}\right]s_{i4}^2(k+1)\\
&+\left[\sigma_{i4}(\lambda_{i4}\sigma_{i4}+\Delta_t\bar{g}_{i4}\bar{\iota}_{i3}\lambda_{i4}\sigma_{i4}-1)+(1-k_{i4})^2\right]\|\hat{\eta}_{i4}(k)\|^2\\
&-\textstyle\sum_{j=2}^{4}\sigma_{ij}\left\|\tilde{\eta}_{ij}(k)\right\|^2+\sum\limits_{j=2}^{4}\sigma_{ij}\left\|\eta_{ij}^*(k)\right\|^2\\
&+\tfrac{\Delta_t\bar{g}_{i2}}{\lambda_{i2}}\bar{\varepsilon}_{i2}^2+\tfrac{\Delta_t\bar{g}_{i3}\bar{\iota}_{i1}}{\lambda_{i3}}\bar{\varepsilon}_{i3}^2+\tfrac{\Delta_t\bar{g}_{i4}\bar{\iota}_{i3}}{\lambda_{i4}}\bar{\varepsilon}_{i4}^2\\
&+3M_{1i}^2+(\upsilon_{2i}+1)M_{2i}^2+(\upsilon_{3i}+1)M_{3i}^2. \qquad \text{(A39)}
\end{aligned}
$$

According to (32) and (48), Equation (A39) can be rewritten as:

$$
\begin{aligned}
\Delta V_i(k)\le&-s_{i1}^2(k)-\left(\tfrac{1}{\Delta_t\bar{g}_{i2}}-3\Delta_t^2-\tfrac{\Delta_t\bar{g}_{i2}k_{ii2}^2}{\lambda_{i2}}\right)s_{i2}^2(k)\\
&-\left(\tfrac{1}{\Delta_t\bar{g}_{i3}\bar{\iota}_{i1}}-\tfrac{\Delta_t\bar{g}_{i2}}{\lambda_{i2}}\right)s_{i3}^2(k)+\left(\tfrac{\upsilon_{3i}b_{i3}^2+b_{i3}^2}{\upsilon_{3i}\tau_{3i}^2}-\frac{1}{2}\right)y_{i3}^2(k)\\
&-\tfrac{1}{\Delta_t\bar{g}_{i4}\bar{\iota}_{i3}}s_{i4}^2(k)+\left(\tfrac{\upsilon_{2i}b_{i2}^2+b_{i2}^2}{\upsilon_{2i}\tau_{2i}^2}-1+3\Delta_t^2\right)y_{i2}^2(k)\\
&-\left[1-3\lambda_{i2}-\lambda_{i2}l_{i2}-\Delta_t\bar{g}_{i2}(\lambda_{i2}l_{i2}+2l_{i2}+2)\right]\tfrac{s_{i2}^2(k+1)}{\Delta_t\bar{g}_{i2}}\\
&-\left[\sigma_{i2}(1-\lambda_{i2}\sigma_{i2}-\Delta_t\bar{g}_{i2}\lambda_{i2}\sigma_{i2})-(1+k_{i2})^2/2\right]\|\hat{\eta}_{i2}(k)\|^2\\
&-\left[1-\lambda_{i3}-\lambda_{i3}l_{i3}-\Delta_t\bar{g}_{i3}\bar{\iota}_{i1}(\lambda_{i3}+1)l_{i3}\right]\frac{s_{i3}^2(k+1)}{\Delta_t\bar{g}_{i3}\bar{\iota}_{i1}}\\
&-\left[\sigma_{i3}(1-\lambda_{i3}\sigma_{i3}-\Delta_t\bar{g}_{i3}\bar{\iota}_{i1}\lambda_{i3}\sigma_{i3})-(1-k_{i3})^2\right]\|\hat{\eta}_{i3}(k)\|^2\\
&-\left[1-\lambda_{i4}-\lambda_{i4}l_{i4}-\Delta_t\bar{g}_{i4}\bar{\iota}_{i3}(\lambda_{i4}+1)l_{i4}\right]\tfrac{s_{i4}^2(k+1)}{\Delta_t\bar{g}_{i4}\bar{\iota}_{i3}}\\
&-\left[\sigma_{i4}(1-\lambda_{i4}\sigma_{i4}-\Delta_t\bar{g}_{i4}\bar{\iota}_{i3}\lambda_{i4}\sigma_{i4})-(1-k_{i4})^2\right]\|\hat{\eta}_{i4}(k)\|^2\\
&+\beta_{i1}+\beta_{i2}+\beta_{i3}+\beta_{i4}, \qquad \text{(A40)}
\end{aligned}
$$

with: $\beta_{i1}=3M_{1i}^2$, $\beta_{i2}=-\sigma_{i2}\|\tilde{\eta}_{i2}(k)\|^2+\sigma_{i2}\left\|\eta_{i2}^*(k)\right\|^2+\frac{\Delta_t\bar{g}_{i2}}{\lambda_{i2}}\bar{\varepsilon}_{i2}^2+(\upsilon_{2i}+1)M_{2i}^2$, $\beta_{i3}=-\sigma_{i3}\|\tilde{\eta}_{i3}(k)\|^2+\sigma_{i3}\left\|\eta_{i3}^*(k)\right\|^2+\frac{\Delta_t\bar{g}_{i3}\bar{\iota}_{i1}}{\lambda_{i3}}\bar{\varepsilon}_{i3}^2+(\upsilon_{3i}+1)M_{3i}^2$, $\beta_{i4}=-\sigma_{i4}\|\tilde{\eta}_{i4}(k)\|^2+\sigma_{i4}\left\|\eta_{i4}^*(k)\right\|^2+\frac{\Delta_t\bar{g}_{i4}\bar{\iota}_{i3}}{\lambda_{i4}}\bar{\varepsilon}_{i4}^2$.

$$
\begin{aligned}
1-3\lambda_{i2}-\lambda_{i2}l_{i2}-\Delta_t\bar{g}_{i2}(\lambda_{i2}l_{i2}+2l_{i2}+2)&\ge 0, &\text{(A41)}\\
1-\lambda_{i3}-\lambda_{i3}l_{i3}-\Delta_t\bar{g}_{i3}\bar{\iota}_{i1}(\lambda_{i3}+1)l_{i3}&\ge 0, &\text{(A42)}\\
1-\lambda_{i4}-\lambda_{i4}l_{i4}-\Delta_t\bar{g}_{i4}\bar{\iota}_{i3}(\lambda_{i4}+1)l_{i4}&\ge 0, &\text{(A43)}\\
\sigma_{i2}(1-\lambda_{i2}\sigma_{i2}-\Delta_t\bar{g}_{i2}\lambda_{i2}\sigma_{i2})-(1+k_{i2})^2/2&\ge 0, &\text{(A44)}\\
\sigma_{i3}(1-\lambda_{i3}\sigma_{i3}-\Delta_t\bar{g}_{i3}\bar{\iota}_{i1}\lambda_{i3}\sigma_{i3})-(1-k_{i3})^2&\ge 0, &\text{(A45)}\\
\sigma_{i4}(1-\lambda_{i4}\sigma_{i4}-\Delta_t\bar{g}_{i4}\bar{\iota}_{i3}\lambda_{i4}\sigma_{i4})-(1-k_{i4})^2&\ge 0, &\text{(A46)}\\
\tfrac{\upsilon_{2i}b_{i2}^2+b_{i2}^2}{\upsilon_{2i}\tau_{i2}^2}-1+3\Delta_t^2\le 0,\quad \tfrac{\upsilon_{3i}b_{i3}^2+b_{i3}^2}{\upsilon_{3i}\tau_{i3}^2}-\frac{1}{2}&\le 0 &\text{(A47)}
\end{aligned}
$$

By selecting the appropriate Δ_t and design parameters, the inequalities (A41)–(A47) hold, which implies that $s_{i1}^2(k) > \beta_{i1}, s_{i2}^2(k) > \frac{\Delta_t \bar{g}_{i2}\lambda_{i2}\beta_{i2}}{\lambda_{i2}-3\Delta_t^3\bar{g}_{i2}\lambda_{i2}-\Delta_t^2\bar{g}_{i2}^2k_{ii2}^2}$, $s_{i3}^2(k) > \frac{\Delta_t \bar{g}_{i3}\bar{\iota}_{i1}\beta_{i3}\lambda_{i2}}{\lambda_{i2}-\Delta_t\bar{g}_{i3}\bar{\iota}_{i1}\Delta_t\bar{g}_{i2}}$, $s_{i4}^2(k) > \Delta_t\bar{g}_{i4}\bar{\iota}_{i3}\beta_{i4}$; then, $\Delta V_i(k) \leq 0$. The proof of Theorem 1 is complete.

References

1. Zhang, X.; Wang, S.; Zhu, G.; Ma, J.; Li, X.; Chen, X. Decentralized robust adaptive neural dynamic surface control for multi-machine excitation systems with static var compensator. *Int. J. Adapt. Control. Signal Process.* **2019**, *33*, 92–113.
2. Zhao, J.; Zheng, Z.; Wang, S.; Huang, R.; Bi, T.; Mili, L.; Huang, Z. Correlation-aided robust decentralized dynamic state estimation of power systems with unknown control inputs. *IEEE Trans. Power Syst.* **2019**, *35*, 2443–2451.
3. Wang, Y.; Feng, G.; Cheng, D.; Liu, Y. Adaptive L2 disturbance attenuation control of multi-machine power systems with SMES units. *Automatica* **2006**, *42*, 1121–1132.
4. Wang, Y.; Guo, G.; Hill, D.J. Robust decentralized nonlinear controller design for multimachine power systems. *Automatica* **1997**, *33*, 1725–1733.
5. Cho, C.S.; Chung, W.H.; Kuo, S.Y. Cyberphysical security and dependability analysis of digital control systems in nuclear power plants. *IEEE Trans. Syst. Man Cybern. Syst.* **2016**, *46*, 356–369.
6. Wang, Z.; Wang, J.; La Scala, M. A Novel Distributed-Decentralized Fixed-Time Optimal Frequency and Excitation Control Framework in a Nonlinear Network-Preserving Power System. *IEEE Trans. Power Syst.* **2020**, *36*, 1285–1297.
7. Hu, J.X.; Jia, Y.; Yin, Q.H. Implementation of DSP Based on Vector Control Model of AC Excitation Control System for a New Hybrid Excitation Synchronous Generator. *Appl. Mech. Mater.* **2015**, *740*, 331–334.
8. Wright, A.D.; Balas, M.J. Design of State-Space-Based Control Algorithms for Wind Turbine Speed Regulation. *J. Sol. Energy-Eng.-Trans. ASME* **2002**, *125*, 386–395.
9. Su, Q.; Quan, W.; Cai, G.; Li, J. An improved adaptive backstepping approach on static var compensator controller of nonlinear power systems. *Int. J. Adapt. Control. Signal Process.* **2018**, *32*, 700–712.
10. Guo, Y.; Hill, D.J.; Wang, Y. Nonlinear decentralized control of large-scale power systems. *Automatica* **2000**, *36*, 1275–1289.
11. Zhu, G.; Nie, L.; Lv, Z.; Sun, L.; Zhang, X.; Wang, C. Adaptive fuzzy dynamic surface sliding mode control of large-scale power systems with prescribe output tracking performance. *ISA Trans.* **2020**, *99*, 305–321.
12. Lu, Q.; Mei, S.; Hu, H.; Wu, F.F.; Ni, Y.; Shen, T. Nonlinear decentralized disturbance attenuation excitation control via new recursive design for multi-machine power systems. *IEEE Trans. Power Syst.* **2001**, *21*, 729–736.
13. Mehraeen, S.; Jagannathan, S.; Crow, M.L. Power system stabilization using adaptive neural network-based dynamic surface control. *IEEE Trans. Power Syst.* **2010**, *26*, 669–680.
14. Jing, Z.; Wen, C.; Yang, G.H. Adaptive Backstepping Stabilization of Nonlinear Uncertain Systems With Quantized Input Signal. *IEEE Trans. Autom. Control* **2014**, *59*, 460–464.
15. Ioannou, P.A. Decentralized adaptive control of interconnected systems. *IEEE Trans. Autom. Control* **1986**, *31*, 291–298.
16. Liu, H.; Hu, Z.; Song, Y. Lyapunov-based decentralized excitation control for global asymptotic stability and voltage regulation of multi-machine power systems. *IEEE Trans. Power Syst.* **2012**, *27*, 2262–2270.
17. Zhang, X.; Wang, Y.; Chen, X.; Su, C.Y.; Li, Z.; Wang, C.; Peng, Y. Decentralized Adaptive Neural Approximated Inverse Control for a Class of Large-Scale Nonlinear Hysteretic Systems with Time Delays. *IEEE Trans. Syst. Man Cybern. Syst.* **2019**, *49*, 2424–2437.
18. Wan, Y.; Milano, F. Nonlinear adaptive excitation control for structure preserving power systems. *IEEE Trans. Power Syst.* **2017**, *33*, 3107–3117.
19. Jiang, Z. Decentralized and adaptive nonlinear tracking of large-scale systems via output feedback. *IEEE Trans. Autom. Control* **2000**, *45*, 2122–2128.
20. Zhang, T.; Xia, X. Decentralized adaptive fuzzy output feedback control of stochastic nonlinear large-scale systems with dynamic uncertainties. *Inf. Sci.* **2015**, *315*, 17–38.
21. Dong, L.; Zhang, Y.; Gao, Z. A robust decentralized load frequency controller for interconnected power systems. *ISA Trans.* **2012**, *51*, 410–419.
22. Wang, Z.; Liu, L.; Li, T.; Zhang, H. Minimum-learning-parameters-based adaptive neural fault tolerant control with its application to continuous stirred tank reactor. *IEEE Trans. Syst. Man Cybern. Syst.* **2020**, *50*, 1275–1285.
23. Zhou, F.; Liu, L.; Feng, G. Fuzzy Decentralized Control for a Class of Networked Systems with Time Delay and Missing Measurements. *Asian J. Control* **2015**, *17*, 84–98.
24. Yang, C.; Jiang, Y.; He, W.; Na, J.; Li, Z.; Xu, B. Adaptive parameter estimation and control design for robot manipulators with finite-time convergence. *IEEE Trans. Ind. Electron.* **2018**, *65*, 8112–8123.
25. Zhang, X.; Chen, X.; Zhu, G.; Su, C.Y. Output Feedback Adaptive Motion Control and Its Experimental Verification for Time-Delay Nonlinear Systems with Asymmetric Hysteresis. *IEEE Trans. Ind. Electron.* **2020**, *67*, 6824–6834.
26. Li, Z.; Shan, J.; Gabbert, U. Dynamics Modeling and Inversion-Based Synchronized Model Predictive Control for a Fabry–Perot Spectrometer. *IEEE/ASME Trans. Mechatron.* **2019**, *24*, 1818–1828.
27. Wang, C.; Wen, C.; Lin, Y.; Wang, W. Decentralized adaptive tracking control for a class of interconnected nonlinear systems with input quantization. *Automatica* **2017**, *81*, 359–368.

28. Liu, Y.; Zhang, H.; Yu, R.; Xing, Z. *H_∞* Tracking Control of Discrete-Time System With Delays via Data-Based Adaptive Dynamic Programming. *IEEE Trans. Syst. Man Cybern. Syst.* **2020**, *50*, 4078–4085.
29. Yeh, P.; Kokotovic, P.V. Adaptive control of a class of nonlinear discrete-time systems. *Int. J. Control* **1995**, *62*, 303–324.
30. Zhang, X.; Li, B.; Chen, X.; Li, Z.; Peng, Y.; Su, C.Y. Adaptive Implicit Inverse Control for a Class of Discrete-Time Hysteretic Nonlinear Systems and Its Application. *IEEE Trans. Mechatron.* **2020**, *25*, 2112–2122.
31. Liu, Y.J.; Li, S.; Tong, S.; Chen, C.P. Adaptive reinforcement learning control based on neural approximation for nonlinear discrete-time systems with unknown nonaffine dead-zone input. *IEEE Trans. Neural Netw. Learn. Syst.* **2019**, *30*, 295–305.
32. Zhang, Y.; Wen, C.; Soh, Y.C. Brief Robust adaptive control of uncertain discrete-time systems. *Automatica* **1999**, *35*, 321–329.
33. Zhang, Y.; Wen, C.; Soh, Y.C. Discrete-time robust backstepping adaptive control for nonlinear time-varying systems. *IEEE Trans. Autom. Control* **2000**, *45*, 1749–1755.
34. Ge, S.S.; Li, G.; Lee, T.H. Adaptive NN control for a class of strict-feedback discrete-time nonlinear systems. *Automatica* **2003**, *39*, 807–819.
35. Zhang, X.; Xu, Z.; Su, C.Y.; Li, Z.; Li, X.; Xiong, C.; Lin, Y. Fuzzy approximator based adaptive dynamic surface control for unknown time delay nonlinear systems with input asymmetric hysteresis nonlinearities. *IEEE Trans. Syst. Man Cybern. Syst.* **2017**, *47*, 2218–2232.
36. Ge, S.S.; Yang, C.; Dai, S.; Jiao, Z.; Lee, T.H. Robust adaptive control of a class of nonlinear strict-feedback discrete-time systems with exact output tracking. *Automatica* **2009**, *45*, 2537–2545.
37. Alanis, A.Y.; Sanchez, E.N.; Loukianov, A.G. Discrete-time adaptive backstepping nonlinear control via high-order neural networks. *IEEE Trans. Neural Netw.* **2007**, *18*, 1185–1195.
38. Liu, Y.J.; Tang, L.; Tong, S.; Chen, C.L. Adaptive NN Controller Design for a Class of Nonlinear MIMO Discrete-Time Systems. *IEEE Trans. Neural Netw. Learn. Syst.* **2015**, *26*, 1007–1018.
39. Yu, J.; Shi, P.; Yu, H.; Chen, B.; Lin, C. Approximation-Based Discrete-Time Adaptive Position Tracking Control for Interior Permanent Magnet Synchronous Motors. *IEEE Trans. Cybern.* **2015**, *45*, 1363–1371.
40. Wu, H.; Liu, Z.; Zhang, Y.; Chen, C.L.P. Adaptive Fuzzy Quantized Control for Nonlinear Systems With Hysteretic Actuator Using a New Filter-Connected Quantizer. *IEEE Trans. Cybern.* **2020**, *50*, 876–889. https://doi.org/10.1109/TCYB.2018.2864166.
41. Xie, K.; Lyu, Z.; Liu, Z.; Zhang, Y.; Chen, C.P. Adaptive Neural Quantized Control for a Class of MIMO Switched Nonlinear Systems With Asymmetric Actuator Dead-Zone. *IEEE Trans. Neural Netw. Learn. Syst.* **2020**, *31*, 1927–1941.
42. Chang, X.; Xiong, J.; Li, Z.; Park, J.H. Quantized Static Output Feedback Control For Discrete-Time Systems. *IEEE Trans. Ind. Inform.* **2017**, *14*, 3426–3435.
43. Wang, C.; Wen, C.; Hu, Q.; Wang, W.; Zhang, X. Distributed Adaptive Containment Control for a Class of Nonlinear Multiagent Systems With Input Quantization. *IEEE Trans. Neural Netw. Learn. Syst.* **2018**, *29*, 2419–2428.
44. Xing, L.; Wen, C.; Yang, Z.; Su, H.; Liu, Z. Output feedback control for uncertain nonlinear systems with input quantization. *Automatica* **2016**, *65*, 191–202.
45. Hayakawa, T.; Ishii, H.; Tsumura, K. Adaptive quantized control for linear uncertain discrete-time systems. *Automatica* **2009**, *45*, 692–700.
46. Li, Y.; Tong, S. Prescribed performance adaptive fuzzy output-feedback dynamic surface control for nonlinear large-scale systems with time delays. *Inf. Sci.* **2015**, *292*, 125–142.
47. Wang, Y.; Zhang, X.; Li, Z.; Chen, X.; Su, C.Y. Adaptive Implicit Inverse Control for a Class of Butterfly-Like Hysteretic Nonlinear Systems and Its Application to Dielectric Elastomer Actuators. *IEEE Trans. Ind. Electron.* **2022**.
48. Sun, L.Y.; Tong, S.; Liu, Y. Adaptive Backstepping Sliding Mode *H_∞* Control of Static Var Compensator. *IEEE Trans. Control. Syst. Technol.* **2010**, *19*, 1178–1185.
49. Xu, W.; Li, Z.; Cui, G.; Wang, C.; Hu, F. Fuzzy adaptive finite time command filter backstepping control of power system. *Int. J. Control. Autom. Syst.* **2021**, *19*, 3812–3822.
50. Wang, S.; Ou, X.; Li, D.; Wang, H.; Zhu, G. K-Filter Observer Based Adaptive Quantized Decentralized Excitation Control for Multi-Machine Power Systems with the Line Transmission Delays. *IEEE Access* **2021**, *9*, 51355–51367.